SIAM J. APPL. MATH.
Vol. 82, No. 2, pp. 694–719

ONE-DIMENSIONAL FERRONEMATICS IN A CHANNEL: ORDER RECONSTRUCTION, BIFURCATIONS, AND MULTISTABILITY*

JAMES DALBY†, PATRICK E. FARRELL‡, APALA MAJUMDAR†, AND JINGMIN XIA§

Abstract. We study a model system with nematic and magnetic order, within a channel geometry modeled by an interval, $[-D, D]$. The system is characterized by a tensor-valued nematic order parameter $\mathbf{Q}$ and a vector-valued magnetization $\mathbf{M}$, and the observable states are modeled as stable critical points of an appropriately defined free energy which includes a nemato-magnetic coupling term, characterized by a parameter c. We (i) derive L^∞ bounds for $\mathbf{Q}$ and $\mathbf{M}$; (ii) prove a uniqueness result in specified parameter regimes; (iii) analyze order reconstruction solutions, possessing domain walls, and their stabilities as a function of D and c and; (iv) perform numerical studies that elucidate the interplay of c and D for multistability.

Key words. liquid crystals, ferronematics, order reconstruction, stability, bifurcations

AMS subject classifications. 34D20, 34C23, 76A15

DOI. 10.1137/21M1400171

1. Introduction.

Nematic liquid crystals (NLCs) are classical examples of mesophases that combine fluidity with long-range orientational order [13]. NLC molecules tend to align, on average, along certain locally preferred directions, referred to as nematic *directors*. NLCs are anisotropic materials with a direction-dependent response to light and external fields, and are thus used in a range of electro-optical devices, e.g., the multibillion dollar liquid crystal display industry [18]. Moreover, NLCs typically rely on their dielectric anisotropy, i.e., directional response to external electric fields, for applications. Their responses to external magnetic fields are much weaker (perhaps seven orders of magnitude smaller) than their dielectric response [27] and consequently, nemato-magnetic coupling has been poorly exploited for NLC applications, e.g., sensors, displays, microfluidics, etc.

In the pioneering work of [7], Brochard and de Gennes suggested that a suspension of magnetic nanoparticles (MNPs) in an NLC host could induce a spontaneous magnetization without any external magnetic fields, and substantially enhance nemato-magnetic material response. This new class of materials with both nematic and magnetic order is referred to as *ferronematics*, with notable theoretical contributions by [9, 10] and experimental realizations by [26], later by [24] where the crucial factors for the stability of ferronematic suspensions are identified. Ferronematics have tremendous potential, both theoretically and for metamaterials, topological

*Received by the editors February 22, 2021; accepted for publication (in revised form) November 4, 2021; published electronically April 27, 2022.
https://doi.org/10.1137/21M1400171
Funding: The work of the second author was supported by the Engineering and Physical Sciences Research Council via grants EP/R029423/1 and EP/V001493/1. The work of the first and third authors was supported by a DST-UKIERI grant. The work of the third author was supported by a Leverhulme International Academic Fellowship, the University of Strathclyde's New Professor Fund, and an OCIAM Visiting Fellowship. The work of the fourth author was supported by the EPSRC Centre for Doctoral Training in Partial Differential Equations via grant, EP/L015811/1 and by the National University of Defense Technology.
†Department of Mathematics, University of Strathclyde, Glasgow, UK (james.dalby@strath.ac.uk, apala.majumdar@strath.ac.uk).
‡Mathematical Institute, University of Oxford, Oxford, UK (patrick.farrell@maths.ox.ac.uk).
§College of Meteorology and Oceanography, National University of Defense Technology, Changsha, China (jingmin.xia@maths.ox.ac.uk).

materials, and nanosystems, to name a few [20]. Of particular interest are multistable ferronematic systems that support multiple stable ferronematic states, without external magnetic fields. This is analogous to multistable nematic systems, such as bistable liquid crystal displays, but ferronematics have additional magnetic order that allows for greater complexity of solution landscapes. This work is a first step in the rigorous analytical and numerical study of multistable one-dimensional ferronematic systems, without external magnetic fields. Magnetic fields could be used to switch between the distinct stable ferronematic states, to control nonequilibrium behavior for such multistable systems.

In this work, we study a dilute suspension of MNPs in a one-dimensional NLC-filled channel (of width D). We assume a uniform distribution of MNPs (much smaller than the physical domain dimensions) such that the average distance between the MNPs is much larger than the MNP size, and the total volume fraction of MNPs is small. These MNPs generate a spontaneous magnetization even without any external magnetic fields, by means of the NLC-MNP interactions. Thus, the system has two order parameters: (i) a reduced Landau–de Gennes (LdG) nematic tensor parameter $\mathbf{Q}$ with two degrees of freedom, that contains information about the nematic directors and the degree of nematic ordering and (ii) a magnetization vector $\mathbf{M}$ generated by the suspended MNPs.

Following the methods in [4, 5, 10], we model the physically observable $(\mathbf{Q}, \mathbf{M})$-profiles as minimizers of an appropriately defined ferronematic free energy. This free energy consists of three contributions: an LdG-type nematic energy, a magnetization energy and a nemato-magnetic coupling energy. In fact, the free energy essentially builds on the energy in [9], with two differences: we describe the nematic state by an LdG-type order parameter instead of a unit-vector as in [9], and we add the magnetization energy to essentially regularize the problem, i.e., the magnetization energy penalizes sharp jumps or inhomogeneities in $\mathbf{M}$. The LdG tensor order parameter is well suited to capture fractional point defects as in [5] and biaxiality in three dimensions, i.e., primary and secondary nematic directors which are outside the scope of a purely vector-based model as in [9]. Further, as shown in [10] and [11], in the dilute limit, the microscopic details of the MNP properties (shape, size, anchoring on the MNP surfaces, volume fraction, etc.) and the NLC-MNP interactions are homogenized to yield the nemato-magnetic coupling energy, characterized by a coupling parameter $c > 0$. The coupling energy dictates the coalignment between the nematic director and $\mathbf{M}$ and for positive c as in our manuscript, this coupling energy favors that the director and $\mathbf{M}$ be parallel to each other. There are four key phenomenological parameters in the ferronematic free energy as in [5]: l_1 and l_2 which depend on elastic constants, the temperature, and are inversely proportional to D^2; the nemato-coupling parameter c; and a scaling parameter ξ that weighs the relative strength of the nematic and magnetic energies. For dilute systems, ξ is typically small. In addition, we prescribe conflicting Dirichlet conditions for $\mathbf{Q}$ and $\mathbf{M}$, that necessarily generate inhomogeneous ferronematic profiles. The physically relevant choices of the boundary conditions for $\mathbf{M}$ are unclear, but we expect our conclusions to be qualitatively unchanged with Neumann boundary conditions for $\mathbf{M}$.

The pure nematic case, i.e., when $c = 0$, is well understood; see, for example, [12, 19]. We study how the solution landscapes for $c = 0$ are perturbed by the nemato-magnetic coupling energy in the dilute limit, for positive c. In the supplementary material, we compute the *vacuum manifold*, i.e., minimizers of the bulk potential, which is the sum of the Ginzburg–Landau energies for $\mathbf{Q}$ and $\mathbf{M}$ and a nemato-magnetic coupling energy, and the bulk minimizers depend on c and ξ. The bulk minimizers are the spatially homogeneous profiles that would be observed without conflicting

boundary conditions or geometrical frustration and they play a crucial role in our study of this one-dimensional spatially inhomogeneous problem of ferronematics in channel geometries. We next prove the existence of minimizers of the ferronematic free energy (Theorem 2.1) for this model problem, subject to the conflicting Dirichlet boundary conditions for $\mathbf{Q}$ and $\mathbf{M}$. The minimizers (local and global) are candidates for physically observable configurations. We then prove a nontrivial maximum principle (Theorem 2.3) for all critical points of the ferronematic free energy, and we obtain an explicit L^∞ bound for the critical points $(\mathbf{Q}, \mathbf{M})$ in terms of c. This bound strongly depends on our analysis of the vacuum manifold. In particular, this bound reduces to the familiar uncoupled bound for $c = 0$ in [12], with a linear perturbation in c for small c. For large c, the bounds grow linearly with c. This captures the relationship between the $c = 0$ and $c > 0$ cases to some extent. Subsequently, in Theorem 2.5 we prove that the ferronematic energy has a unique critical point, and hence minimizer, for D sufficiently small, i.e., for narrow channels, as for the $c = 0$ case in [19]. Of course, the critical D depends on c. These crucial analytic results hold in two and three dimensions too, and are hence of general interest.

In the pure nematic case ($c = 0$), the model problem admits a unique order reconstruction (OR) solution for $D \ll c_2\xi_n$ for some positive constant c_2 independent of model parameters, and where ξ_n is the nematic correlation length [19]. OR solutions are special since they support polydomains, separated by domain walls, such that the nematic director is constant in each polydomain and jumps across the domain wall. These polydomains are stable for D small enough, and become unstable as D increases. The qualitative features are unchanged in the ferronematic case, where profiles have four degrees of freedom: two for $\mathbf{Q}$ and two for $\mathbf{M}$. Here, an OR solution exists for all D (Theorem 3.1), with distinct domain walls (defined by $\mathbf{Q} = 0$ and $\mathbf{M} = 0$) that separate distinctly ordered polydomains for both the nematic director and the magnetization vector. The OR solutions are reduced solutions with only two degrees of freedom and the polydomains are a necessary consequence of the Dirichlet boundary conditions. Essentially, the polydomains have a constant nonzero $(\mathbf{Q}, \mathbf{M})$-profile and the profile jumps across a domain wall, which is the surface discontinuity in the three-dimensional channel setting. Moreover, OR solutions are globally stable for $D \ll c_1 \frac{\xi_n}{\sqrt{c_0^2+c^2}}$ and thus c shrinks their domain of stability. In Theorem 3.3, as D increases, we show that OR solutions become unstable by means of a Γ-convergence argument and second variation analysis. Next, we study the full problem with four degrees of freedom. As D increases, the ferronematic energy minimizers lose the polydomain structures and the nematic director and the magnetization vector rotate smoothly throughout the channel. For large D, these minimizers exploit the full four degrees of freedom, and we have boundary layers because the boundary conditions are not consistent with the vacuum manifold. This is further corroborated by numerical experiments and computations of bifurcation diagrams, for two specific values of c. As D increases, we observe pitchfork bifurcations from the OR solutions and multiple stable ferronematic equilibria for large D, demonstrating an example of a multistable ferronematic system.

The nemato-magnetic coupling introduces additional possibilities for the interplay between nematic and magnetic domain walls (absent when $c = 0$), new defect structures, and novel bifurcations accompanied by novel solution branches for large D. In particular, the ferronematic OR solutions illustrate how we can tailor the locations and multiplicity of domain walls by varying D and c, a novel aspect of our study. We do not address these questions fully in this manuscript but our work will

support and guide future studies on these lines. The paper is organized as follows. In the next section, we describe the ferronematic model and give some qualitative results of general interest, e.g., existence, uniqueness, etc. We then consider the OR model in section 3 and provide numerical results in section 4 to verify our theoretical analysis. Finally, some conclusions and perspectives are summarized in section 5.

2. Model problem. We consider a dilute ferronematic suspension sandwiched inside the three-dimensional channel $\tilde{\Omega} = [-L, L] \times [-D, D] \times [0, G]$, where $L \gg D$, L is the length of the channel, D is the channel width, and G is the channel height. We impose strong anchoring on the xz-planes and free boundary conditions on the yz- and xy-planes. From a modeling perspective, we assume that the structural profile is invariant across the height of the channel, and along the length of the channel and restrict ourselves to a one-dimensional channel geometry: $\Omega = [-D, D]$ in what follows. As noted from section 1, the ferronematic suspension is described by two order parameters: we have a symmetric, traceless 2×2 matrix $\mathbf{Q}$, i.e., we have $\mathbf{Q} \in S_0 := \{\mathbf{Q} \in \mathbb{M}^{2\times 2} : Q_{ij} = Q_{ji}, Q_{ii} = 0\}$, and a two-dimensional vector, $\mathbf{M} = (M_1, M_2)$. Here, $\mathbb{M}^{2\times 2}$ denotes all 2×2 matrices. The nematic order parameter $\mathbf{Q}$ can be written as

$$\mathbf{Q} = s(2\mathbf{n} \otimes \mathbf{n} - \mathbf{I}), \tag{2.1}$$

where s is a scalar order parameter, and $\mathbf{n}$ is the nematic director (a unit vector describing the direction of orientational ordering in the xy-plane) and $\mathbf{I}$ is the 2×2 identity matrix. Moreover, s is interpreted as the degree of the orientational order about $\mathbf{n}$, so that the nodal sets of s (i.e., where $s = 0$) define nematic defects in the xy-plane. We denote the two independent components of $\mathbf{Q}$ by Q_{11} and Q_{12} such that

$$Q_{11} = s\cos 2\vartheta, \quad Q_{12} = s\sin 2\vartheta,$$

when $\mathbf{n} = (\cos\vartheta, \sin\vartheta)$ and ϑ denotes the angle between $\mathbf{n}$ and the horizontal axis. To avoid writing $\mathbf{Q}$ in the matrix form $\left[\begin{smallmatrix} Q_{11} & Q_{12} \\ Q_{12} & -Q_{11} \end{smallmatrix}\right]$, we henceforth label $\mathbf{Q}$ in terms of its two independent components (Q_{11}, Q_{12}), when this causes no confusions. We therefore define the vector norm, $|\mathbf{Q}| = \sqrt{Q_{11}^2 + Q_{12}^2}$, as opposed to a matrix norm. Similarly, we define $|\mathbf{M}| = \sqrt{M_1^2 + M_2^2}$.

Following the methods in [24, 4], the ferronematic free energy is given by the sum of three energies for low temperatures: an LdG-type nematic energy for $\mathbf{Q}$, a magnetization energy for $\mathbf{M}$, and a coupling energy between $\mathbf{Q}$ and $\mathbf{M}$. For dilute ferronematic suspensions, the MNP interactions are "small" and the NLC-MNP interactions are absorbed by the coupling energy, which can be viewed as the homogenized version of a Rapini–Papoular-type surface anchoring energy on the MNP surfaces that dictates the coalignment between $\mathbf{n}$ and $\mathbf{M}$ [10, 11]. We adopt the rescalings as in [4], so that the rescaled domain is $\Omega = [-1, 1]$, and the total rescaled and dimensionless ferronematic free energy is

$$\begin{aligned} F(Q_{11}, Q_{12}, M_1, M_2) := \int_\Omega \Bigg\{ & \frac{l_1}{2}\left[\left(\frac{\mathrm{d}Q_{11}}{\mathrm{d}y}\right)^2 + \left(\frac{\mathrm{d}Q_{12}}{\mathrm{d}y}\right)^2\right] + \left(Q_{11}^2 + Q_{12}^2 - 1\right)^2 \\ & + \frac{\xi l_2}{2}\left[\left(\frac{\mathrm{d}M_1}{\mathrm{d}y}\right)^2 + \left(\frac{\mathrm{d}M_2}{\mathrm{d}y}\right)^2\right] + \frac{\xi}{4}\left(M_1^2 + M_2^2 - 1\right)^2 \\ & - cQ_{11}\left(M_1^2 - M_2^2\right) - 2cQ_{12}M_1M_2 \Bigg\} \, \mathrm{d}y. \end{aligned} \tag{2.2}$$

Here, $l_1 > 0$ and $l_2 > 0$ are scaled elastic constants (inversely proportional to D^2, i.e., the squared channel width). Substituting (2.1) into the coupling energy, we observe that

$$\left(-cQ_{11}\left(M_1^2 - M_2^2\right) - 2cQ_{12}M_1M_2\right) \propto -c\left(\mathbf{n}\cdot\mathbf{M}\right)^2.$$

We only focus on positive coupling, i.e., $c > 0$ in this work so that this coupling energy favors $\mathbf{n}\cdot\mathbf{M} = \pm 1$. We further denote the bulk energy density by

$$\begin{aligned} f(Q_{11}, Q_{12}, M_1, M_2) \coloneqq &\left(Q_{11}^2 + Q_{12}^2 - 1\right)^2 + \frac{\xi}{4}\left(M_1^2 + M_2^2 - 1\right)^2 \\ &- cQ_{11}\left(M_1^2 - M_2^2\right) - 2cQ_{12}M_1M_2. \end{aligned} \tag{2.3}$$

Regarding boundary conditions, we work with Dirichlet conditions for $\mathbf{Q}$ and $\mathbf{M}$ on the boundaries $y = \pm 1$, i.e.,

$$\begin{aligned} &Q_{11}(-1) = M_1(-1) = 1, \\ &Q_{12}(-1) = Q_{12}(1) = M_2(-1) = M_2(1) = 0, \\ &Q_{11}(1) = M_1(1) = -1. \end{aligned} \tag{2.4}$$

Here, the boundary conditions for $\mathbf{Q}$ correspond to $\mathbf{n} = (1,0)$ on $y = -1$ and $\mathbf{n} = (0,1)$ on $y = 1$, hence, we have planar boundary conditions on $y = -1$ and normal/homeotropic boundary conditions on $y = +1$. Furthermore, the boundary conditions for $\mathbf{M}$ describe a π-rotation between the bounding plates, $y = \pm 1$.

The admissible space is given by

$$\begin{aligned} \mathcal{A} = \big\{&\mathbf{Q} \in W^{1,2}(\Omega; S_0), \mathbf{M} \in W^{1,2}\left(\Omega; \mathbb{R}^2\right), \\ &\mathbf{Q} \text{ and } \mathbf{M} \text{ satisfy the boundary conditions (2.4)}\big\}. \end{aligned} \tag{2.5}$$

The Sobolev space $W^{1,2}$ is the space of all square-integrable $(\mathbf{Q}, \mathbf{M})$ with square-integrable first weak derivatives, which is a standard choice for such variational problems. The stable, physically relevant, and potentially observable $(\mathbf{Q}, \mathbf{M})$-profiles are local or global energy minimizers of the full energy (2.2) subject to the boundary conditions in (2.4), in $\mathcal{A}$. They are in fact, classical solutions of the associated Euler–Lagrange equations [4]

$$l_1\frac{\mathrm{d}^2Q_{11}}{\mathrm{d}y^2} = 4Q_{11}(Q_{11}^2 + Q_{12}^2 - 1) - c\left(M_1^2 - M_2^2\right), \tag{2.6a}$$

$$l_1\frac{\mathrm{d}^2Q_{12}}{\mathrm{d}y^2} = 4Q_{12}(Q_{11}^2 + Q_{12}^2 - 1) - 2cM_1M_2, \tag{2.6b}$$

$$\xi l_2\frac{\mathrm{d}^2M_1}{\mathrm{d}y^2} = \xi M_1\left(M_1^2 + M_2^2 - 1\right) - 2cQ_{11}M_1 - 2cQ_{12}M_2, \tag{2.6c}$$

$$\xi l_2\frac{\mathrm{d}^2M_2}{\mathrm{d}y^2} = \xi M_2\left(M_1^2 + M_2^2 - 1\right) + 2cQ_{11}M_2 - 2cQ_{12}M_1. \tag{2.6d}$$

The first result concerns a brief proof of the existence of a global minimizer of the free energy (2.2), in $\mathcal{A}$.

THEOREM 2.1. *For all positive values of (l_1, l_2, c, ξ), there exists at least one minimizer $(Q_{11}^*, Q_{12}^*, M_1^*, M_2^*)$ of the ferronematic free energy* (2.2) *in the admissible space* (2.5). *Moreover, this minimizer is a (classical) solution of the Euler–Lagrange equations* (2.6a)–(2.6d) *subject to the boundary conditions* (2.4).

Remark 2.2. For brevity of notations, we omit $(\Omega; S_0)$ and $(\Omega; \mathbb{R}^2)$ in the Sobolev spaces hereafter, whenever it causes no confusion.

Proof. The admissible space (2.5) is nonempty as $(Q_{11}, Q_{12}, M_1, M_2) = (-y, 0,$
$-y, 0) \in \mathcal{A}$. The ferronematic energy (2.2) is quadratic and thus, convex in the gradient of all four state variables $(Q_{11}, Q_{12}, M_1, M_2)$ and hence, lower semicontinuous [14]. Furthermore, the coupling energy can be decomposed as follows,

$$\begin{aligned} -cQ_{11}\left(M_1^2 - M_2^2\right) - 2cQ_{12}M_1M_2 &\geq -c(M_1^2 + M_2^2)(|Q_{11}| + |Q_{12}|) \\ &\geq -\frac{c}{2}\left(\epsilon\left(|Q_{11}| + |Q_{12}|\right)^2 + \frac{1}{\epsilon}\left(M_1^2 + M_2^2\right)^2\right) \\ &\geq -\frac{c}{2}\left(2\epsilon\left(Q_{11}^2 + Q_{12}^2\right) + \frac{1}{\epsilon}\left(M_1^2 + M_2^2\right)^2\right), \end{aligned}$$

where $\epsilon > 0$ is arbitrary. Hence, the energy density is bounded from below as

$$\begin{aligned} &\frac{l_1}{2}\left[\left(\frac{\mathrm{d}Q_{11}}{\mathrm{d}y}\right)^2 + \left(\frac{\mathrm{d}Q_{12}}{\mathrm{d}y}\right)^2\right] + \left(Q_{11}^2 + Q_{12}^2 - 1\right)^2 + \frac{\xi l_2}{2}\left[\left(\frac{\mathrm{d}M_1}{\mathrm{d}y}\right)^2 + \left(\frac{\mathrm{d}M_2}{\mathrm{d}y}\right)^2\right] \\ &\quad + \frac{\xi}{4}\left(M_1^2 + M_2^2 - 1\right)^2 - cQ_{11}\left(M_1^2 - M_2^2\right) - 2cQ_{12}M_1M_2 \\ &\geq \frac{l_1}{2}\left[\left(\frac{\mathrm{d}Q_{11}}{\mathrm{d}y}\right)^2 + \left(\frac{\mathrm{d}Q_{12}}{\mathrm{d}y}\right)^2\right] + \frac{\xi l_2}{2}\left[\left(\frac{\mathrm{d}M_1}{\mathrm{d}y}\right)^2 + \left(\frac{\mathrm{d}M_2}{\mathrm{d}y}\right)^2\right] \\ &\quad + \left[Q_{11}^2 + Q_{12}^2 - \left(1 + \frac{c\epsilon}{2}\right)\right]^2 + \left(\frac{\xi\epsilon - 2c}{4\epsilon}\right)\left(M_1^2 + M_2^2 - \frac{\epsilon\xi}{\xi\epsilon - 2c}\right)^2 \\ &\quad - \left(c\epsilon + \frac{c^2\epsilon^2}{4} + \frac{c\xi}{2(\xi\epsilon - 2c)}\right), \end{aligned}$$

and thus the full energy (2.2) is coercive provided $\epsilon > \frac{2c}{\xi}$. The existence of a minimizer in the admissible space $\mathcal{A}$ therefore follows by the direct method in the calculus of variations [14]. We can follow the arguments from elliptic regularity in [3] and [23] to deduce that minimizers, and in fact all critical points of the free energy, are classical solutions of (2.6a)–(2.6d). ∎

2.1. Maximum principle and uniqueness results. For simplicity and brevity, we take $l_1 = l_2 = l$ and $\xi = 1$ hereafter. The cases of $l_1 \neq l_2$ and $\xi \neq 1$ can be tackled using similar mathematical methods, although ξ is necessarily small for dilute ferronematic suspensions.

THEOREM 2.3 (maximum principle). *There exists an L^∞ bound for the solutions, $(Q_{11}, Q_{12}, M_1, M_2)$ of the system* (2.6a)–(2.6d)*, subject to the boundary conditions* (2.4)*. Specifically,*

$$Q_{11}^2(y) + Q_{12}^2(y) \leq (\rho^*)^2,\ M_1^2(y) + M_2^2(y) \leq 1 + 2c\rho^* \quad \forall y \in [-1, 1], \tag{2.7}$$

where ρ^* is given by

$$\rho^* = \left(\frac{c}{8} + \sqrt{\frac{c^2}{64} - \frac{1}{27}\left(1 + \frac{c^2}{2}\right)^3}\right)^{\frac{1}{3}} + \left(\frac{c}{8} - \sqrt{\frac{c^2}{64} - \frac{1}{27}\left(1 + \frac{c^2}{2}\right)^3}\right)^{\frac{1}{3}}. \tag{2.8}$$

Proof. Assume that, $|\mathbf{Q}| = \sqrt{Q_{11}^2 + Q_{12}^2}$ and, $|\mathbf{M}| = \sqrt{M_1^2 + M_2^2}$, attain their maxima at two distinct points $y_1, y_2 \in (-1, 1)$, respectively, then we have

$$\frac{\mathrm{d}^2}{\mathrm{d}y^2}\left(\frac{1}{2}|\mathbf{Q}|^2\right)(y_1) \leq 0 \text{ and } \frac{\mathrm{d}^2}{\mathrm{d}y^2}\left(\frac{1}{2}|\mathbf{M}|^2\right)(y_2) \leq 0.$$

Multiplying (2.6a) by Q_{11}, (2.6b) by Q_{12}, adding the resulting equations, and using the identity $\frac{\mathrm{d}^2}{\mathrm{d}y^2}(\frac{1}{2}|\mathbf{Q}|^2) = \frac{\mathrm{d}^2 Q_{11}}{\mathrm{d}y^2}Q_{11} + \frac{\mathrm{d}^2 Q_{12}}{\mathrm{d}y^2}Q_{12} + (\frac{\mathrm{d}Q_{11}}{\mathrm{d}y})^2 + (\frac{\mathrm{d}Q_{12}}{\mathrm{d}y})^2$, we obtain the necessary condition

(2.9)
$$\left[4\left(Q_{11}^2 + Q_{12}^2\right)\left(Q_{11}^2 + Q_{12}^2 - 1\right) - c\left(Q_{11}\left(M_1^2 - M_2^2\right) + 2Q_{12}M_1M_2\right)\right]\Big|_{y=y_1} \leq 0.$$

Similarly, we have

(2.10)
$$\left[\left(M_1^2 + M_2^2\right)\left(M_1^2 + M_2^2 - 1\right) - 2c\left(Q_{11}(M_1^2 - M_2^2) + 2Q_{12}M_1M_2\right)\right]\Big|_{y=y_2} \leq 0.$$

Substituting

$$\begin{aligned} &Q_{11} = \rho\cos(\theta), Q_{12} = \rho\sin(\theta), \\ &M_1 = \sigma\cos(\phi), M_2 = \sigma\sin(\phi) \end{aligned} \tag{2.11}$$

with $\rho = |\mathbf{Q}| \geq 0$ and $\sigma = |\mathbf{M}| \geq 0$, with arbitrary θ and ϕ, into (2.9) and (2.10), we obtain

$$\begin{aligned} 0 \geq \left[4\rho^2(\rho^2 - 1) - c\rho\sigma^2\cos(\theta - 2\phi)\right]\Big|_{y=y_1} &\geq \left[4\rho^2(\rho^2 - 1) - c\rho\sigma^2\right]\Big|_{y=y_1} \\ \implies \left(\rho^3 - \rho - \frac{c\sigma^2}{4}\right)\Big|_{y=y_1} &\leq 0, \end{aligned} \tag{2.12}$$

and

$$\begin{aligned} 0 \geq \left[\sigma^2(\sigma^2 - 1) - 2c\rho\sigma^2\cos(\theta - 2\phi)\right]\Big|_{y=y_2} &\geq \left[\sigma^2(\sigma^2 - 1) - 2c\rho\sigma^2\right]\Big|_{y=y_2} \\ \implies \left(\sigma^2 - 1 - 2c\rho\right)\Big|_{y=y_2} &\leq 0, \end{aligned}$$

respectively. We then immediately deduce that $\sigma^2(y) \leq 1 + 2c\rho(y_2)$ for all $y \in [-1, 1]$, as $|\mathbf{M}|$ attains its maximum at y_2, and since $\rho(y_1) \geq \rho(y_2)$ (as $|\mathbf{Q}|$ attains its maximum at y_1), we further have $\sigma^2(y_1) \leq 1 + 2c\rho(y_1)$. Using this in (2.12), we get

$$0 \geq \left(\rho^3 - \rho - \frac{c\sigma^2}{4}\right)\Big|_{y=y_1} \geq \left(\rho^3 - \rho\left(1 + \frac{c^2}{2}\right) - \frac{c}{4}\right)\Big|_{y=y_1},$$

which holds provided that ρ is less than or equal to the largest positive root of the cubic polynomial, $\rho^3 - \rho(1 + \frac{c^2}{2}) - \frac{c}{4}$. From the detailed calculations in the supplementary materials, the largest positive root is given by

$$\rho = \left(\frac{c}{8} + \sqrt{\frac{c^2}{64} - \frac{1}{27}\left(1 + \frac{c^2}{2}\right)^3}\right)^{\frac{1}{3}} + \left(\frac{c}{8} - \sqrt{\frac{c^2}{64} - \frac{1}{27}\left(1 + \frac{c^2}{2}\right)^3}\right)^{\frac{1}{3}},$$

and thus $\rho(y_1) \le \rho^*$. The L^∞ bounds for ρ and σ are an immediate consequence, i.e.,

$$\rho(y) \le \rho^*,\ \sigma^2(y) \le 1 + 2c\rho^* \quad \forall y \in [-1,1].$$

Note that if $y_1 = y_2$, the proof is unchanged since $\rho(y_1) = \rho(y_2)$. ∎

Remark 2.4. For $c = 0$, the upper bounds (2.7) reduce to $Q_{11}^2 + Q_{12}^2 \le 1,\ M_1^2 + M_2^2 \le 1$, which are the Ginzburg–Landau bounds in [22] for $\mathbf{Q}$ and $\mathbf{M}$. Moreover, if c is small, we can expand ρ^* in powers of c to deduce that $Q_{11}^2 + Q_{12}^2 \le 1 + \frac{c}{4},\ M_1^2 + M_2^2 \le 1 + 2c$ to leading order in c. Hence, the nemato-magnetic coupling perturbs the Ginzburg–Landau bounds linearly, for small c (see the supplementary material (M140017SupMat.pdf [local/web 443KB]) for the case of large c too).

With the L^∞ bounds at hand, one can prove that there is a unique critical point of (2.2), which is necessarily the global energy minimizer, in the $l \to \infty$ limit.

THEOREM 2.5 (uniqueness of minimizers for sufficiently large l). *For a fixed c and for $l_1 = l_2 =: l$ sufficiently large and $\xi = 1$, there exists a unique critical point (and hence global minimizer) of the full energy* (2.2)*, in the admissible space* (2.5)*.*

Proof. We first show that the free energy (2.2) is strictly convex using the maximum principle. In fact, we let $(\mathbf{Q},\mathbf{M}), (\overline{\mathbf{Q}},\overline{\mathbf{M}}) \in \mathcal{A}$ so that $(\mathbf{Q} - \overline{\mathbf{Q}}) \in W_0^{1,2}$ and $(\mathbf{M} - \overline{\mathbf{M}}) \in W_0^{1,2}$, where $W_0^{1,2}$ is the closure of C_0^∞ with respect to the $W^{1,2}$-norm. Note that

$$\begin{aligned} F\left(\frac{\mathbf{Q}+\overline{\mathbf{Q}}}{2}, \frac{\mathbf{M}+\overline{\mathbf{M}}}{2}\right) =& \frac{1}{2}\left[F(\mathbf{Q},\mathbf{M}) + F(\overline{\mathbf{Q}},\overline{\mathbf{M}})\right] + \int_\Omega \Bigg\{ f\left(\frac{\mathbf{Q}+\overline{\mathbf{Q}}}{2}, \frac{\mathbf{M}+\overline{\mathbf{M}}}{2}\right) \\ & - \frac{1}{2}\left[f(\mathbf{Q},\mathbf{M}) + f(\overline{\mathbf{Q}},\overline{\mathbf{M}})\right] - \frac{l}{8}\left[\left(\frac{\mathrm{d}\mathbf{Q}}{\mathrm{d}y}\right) - \left(\frac{\mathrm{d}\overline{\mathbf{Q}}}{\mathrm{d}y}\right)\right]^2 \\ & - \frac{l}{8}\left[\left(\frac{\mathrm{d}\mathbf{M}}{\mathrm{d}y}\right) - \left(\frac{\mathrm{d}\overline{\mathbf{M}}}{\mathrm{d}y}\right)\right]^2 \Bigg\} \mathrm{d}y \\ \le& \frac{1}{2}\left[F(\mathbf{Q},\mathbf{M}) + F(\overline{\mathbf{Q}},\overline{\mathbf{M}})\right] + \int_\Omega \Bigg\{ f\left(\frac{\mathbf{Q}+\overline{\mathbf{Q}}}{2}, \frac{\mathbf{M}+\overline{\mathbf{M}}}{2}\right) \\ & - \frac{1}{2}\left[f(\mathbf{Q},\mathbf{M}) + f(\overline{\mathbf{Q}},\overline{\mathbf{M}})\right] \Bigg\} \mathrm{d}y - \frac{l}{16}\|\mathbf{Q} - \overline{\mathbf{Q}}\|_{L^2}^2 \\ & - \frac{l}{16}\|\mathbf{M} - \overline{\mathbf{M}}\|_{L^2}^2, \end{aligned} \tag{2.13}$$

where f is the bulk energy density (2.3), and we have used the Poincaré inequality with the Poincaré constant $c_p = \frac{1}{2}$ in the last inequality. We estimate the second partial derivatives of f, using the L^∞ bounds above, yielding

$$\begin{aligned} &\frac{\partial^2 f}{\partial Q_{1i}\partial Q_{1j}} = 4\delta_{ij}\left(Q_{11}^2 + Q_{12}^2 - 1\right) + 8Q_{1i}Q_{1j} \le 4\left(3(\rho^*)^2 - 1\right) =: a_1, \\ &\left|\frac{\partial^2 f}{\partial M_i \partial M_j}\right| \le B(5c\rho^* + 1) =: a_2, \\ &\left|\frac{\partial^2 f}{\partial Q_{1i}\partial M_j}\right| \le Ac\sqrt{1 + 2c\rho*} =: a_3 \end{aligned}$$

for $i, j \in \{1, 2\}$, where δ_{ij} is the Kronecker delta symbol and A, B are constants independent of c. Using methods parallel to [19, Lemma 8.2], we have

$$\int_\Omega \left\{ f\left(\frac{\mathbf{Q}+\overline{\mathbf{Q}}}{2}, \frac{\mathbf{M}+\overline{\mathbf{M}}}{2}\right) - \frac{1}{2}\left[f(\mathbf{Q},\mathbf{M}) + f\left(\overline{\mathbf{Q}},\overline{\mathbf{M}}\right)\right] \right\} \mathrm{d}y \\ \leq a_1\|\mathbf{Q}-\overline{\mathbf{Q}}\|_{L^2}^2 + a_2\|\mathbf{M}-\overline{\mathbf{M}}\|_{L^2}^2 + a_3\|\mathbf{Q}-\overline{\mathbf{Q}}\|_{L^2}\|\mathbf{M}-\overline{\mathbf{M}}\|_{L^2}. \tag{2.14}$$

Note that

$$\left\|\mathbf{Q}-\overline{\mathbf{Q}}\right\|_{L^2}\left\|\mathbf{M}-\overline{\mathbf{M}}\right\|_{L^2} \leq \frac{1}{2}\left(\epsilon\left\|\mathbf{Q}-\overline{\mathbf{Q}}\right\|_{L^2}^2 + \epsilon^{-1}\left\|\mathbf{M}-\overline{\mathbf{M}}\right\|_{L^2}^2\right) \quad \forall \epsilon > 0.$$

We take $\epsilon = 2$ for convenience and then substitute (2.14) into (2.13), so that

$$F\left(\frac{\mathbf{Q}+\overline{\mathbf{Q}}}{2}, \frac{\mathbf{M}+\overline{\mathbf{M}}}{2}\right) \leq \frac{1}{2}\left[F(\mathbf{Q},\mathbf{M}) + F\left(\overline{\mathbf{Q}},\overline{\mathbf{M}}\right)\right] + \left(a_1 + a_3 - \frac{l}{16}\right)\|\mathbf{Q}-\overline{\mathbf{Q}}\|_{L^2}^2 \\ + \left(a_2 + \frac{a_3}{4} - \frac{l}{16}\right)\|\mathbf{M}-\overline{\mathbf{M}}\|_{L^2}^2.$$

Hence, for $l > l^*(c) = \max\{16(a_1+a_3), 4(4a_2+a_3)\}$, it holds that

$$F\left(\frac{\mathbf{Q}+\overline{\mathbf{Q}}}{2}, \frac{\mathbf{M}+\overline{\mathbf{M}}}{2}\right) < \frac{1}{2}F(\mathbf{Q},\mathbf{M}) + \frac{1}{2}F\left(\overline{\mathbf{Q}},\overline{\mathbf{M}}\right)$$

for all $\mathbf{Q}, \overline{\mathbf{Q}} \in W^{1,2}$ and $\mathbf{M}, \overline{\mathbf{M}} \in W^{1,2}$ such that $\mathbf{Q} \neq \overline{\mathbf{Q}}$, $\mathbf{M} \neq \overline{\mathbf{M}}$. Therefore, F is strictly convex.

Now assume that for $l \in (l^*, \infty)$, there exist two solutions $(\mathbf{Q}, \mathbf{M})$ and $\left(\overline{\mathbf{Q}}, \overline{\mathbf{M}}\right)$ of (2.6a)–(2.6d) in the admissible space $\mathcal{A}$. Then the mapping

$$[0,1] \ni t \mapsto F\left(t\mathbf{Q} + (1-t)\overline{\mathbf{Q}}, t\mathbf{M} + (1-t)\overline{\mathbf{M}}\right)$$

is C^1 (continuously differentiable) and its derivative vanishes at $t = 0, 1$. However, this contradicts the strict convexity of F and hence, the uniqueness result follows. ∎

Remark 2.6. The existence, uniqueness, and maximum principle results work in two and three dimensions, and can be adapted to $l_1 \neq l_2$ and $\xi \neq 1$. Recall the definitions of the dimensionless parameters in [4]:

$$l_1 = \frac{L}{D^2|A|},\ l_2 = \frac{\kappa}{D^2|\alpha|},\ c = \frac{\gamma\mu_0}{|A|}\sqrt{\frac{C}{2|A|}}\frac{|\alpha|}{\beta}, \tag{2.15}$$

where A is the rescaled temperature, L is the nematic elastic constant, κ is the magnetic elastic constant, C, α, β are material-dependent constants, γ is a coupling parameter, and μ_0 is a universal constant. From Theorem 2.5, the conditions $l = l_1 = l_2 > l^*(c) = \max\{16(a_1+a_3), 4(4a_2+a_3)\}$ guarantee the uniqueness of a solution for the system (2.6a)–(2.6d). The parameters a_1, a_2, a_3 grow as c^2 for large c, and thus the condition $l > l^*(c)$ is equivalent to $\frac{c_1^2 L}{D^2|A|(c_0^2+c^2)} \gg 1$ for some constants c_0, c_1 or $D \ll \sqrt{\frac{c_1^2 L}{|A|(c_0^2+c^2)}} =: c_1\frac{\xi_n}{\sqrt{c_0^2+c^2}}$, i.e., when the physical length D is much smaller than an enhanced material-dependent length scale $c_1\frac{\xi_n}{\sqrt{c_0^2+c^2}}$. Here, $\xi_n = \sqrt{\frac{L}{|A|}}$ is the temperature-dependent nematic correlation length. For $c = 0$, we recover the uniqueness results reported in [19] and [12].

2.2. Convergence analysis for $l \to \infty$ and $l \to 0$. For a fixed $c > 0$, the $l \to \infty$ limit corresponds to very narrow channels with $D \ll \sqrt{\frac{L}{|A|(c_0^2+c^2)}}$ as discussed in Remark 2.6. From the maximum principle Theorem 2.3, $\|\mathbf{Q}\|_{L^\infty}$ and $\|\mathbf{M}\|_{L^\infty}$ are bounded independently of l, as shown in (2.7). Furthermore, in the $l \to \infty$ limit, one can easily see that (2.6a)-(2.6d) reduce to the Laplace equations

$$\begin{aligned} &\frac{\mathrm{d}^2 Q_{11}}{\mathrm{d}y^2} = 0, \quad \frac{\mathrm{d}^2 Q_{12}}{\mathrm{d}y^2} = 0, \\ &\frac{\mathrm{d}^2 M_1}{\mathrm{d}y^2} = 0, \quad \frac{\mathrm{d}^2 M_2}{\mathrm{d}y^2} = 0, \end{aligned} \tag{2.16}$$

subject to (2.4), which admits the unique solution as shown below:

$$(\mathbf{Q}^\infty, \mathbf{M}^\infty) = (Q_{11}^\infty, Q_{12}^\infty, M_1^\infty, M_2^\infty) = (-y, 0, -y, 0). \tag{2.17}$$

In fact, (2.17) is an OR solution, as introduced in section 3, with linear profiles for Q_{11} and M_1. In the next theorem, we use the method of sub- and super-solutions as in [15] to study the convergence of solutions of (2.6a)–(2.6d) to $(\mathbf{Q}^\infty, \mathbf{M}^\infty)$, as $l \to \infty$.

THEOREM 2.7 (convergence result for $l \to \infty$). *Assume $l > l^*$. Let $(\mathbf{Q}^l, \mathbf{M}^l)$ be the unique solution of the Euler–Lagrange equations* (2.6a)–(2.6d) *in* (2.5). *Then $(\mathbf{Q}^l, \mathbf{M}^l)$ converge to $(\mathbf{Q}^\infty, \mathbf{M}^\infty)$ as $l \to \infty$, with the following estimates,*

$$\forall j = 1, 2, \quad \|Q_{1j}^l - Q_{1j}^\infty\|_{L^\infty} \le \alpha_1 l^{-1}, \ \|M_j^l - M_j^\infty\|_{L^\infty} \le \alpha_2 l^{-1} \tag{2.18}$$

for positive constants α_1, α_2 independent of l.

Proof. Recalling [15, Proposition 3.1] and comparing (2.6a)–(2.6d) with the Laplace equations (2.16), we have for $j = 1, 2$,

(2.19a)

$$\begin{aligned} -l^{-1}\left(4\rho^*\left((\rho^*)^2 - 1\right) + c\,(1 + 2c\rho^*)\right) &\le \frac{\mathrm{d}^2}{\mathrm{d}y^2}\left(Q_{1j}^l - Q_{1j}^\infty\right) \\ &\le l^{-1}\left(4\rho^*\left((\rho^*)^2 - 1\right) + c\,(1 + 2c\rho^*)\right) \quad \text{in } \Omega, \end{aligned}$$

$$Q_{1j}^l - Q_{1j}^\infty = 0 \ \text{ on } \partial\Omega, \tag{2.19b}$$

(2.19c)

$$-l^{-1} 6c\rho^* (1 + 2c\rho^*)^{\frac{1}{2}} \le \frac{\mathrm{d}^2}{\mathrm{d}y^2}(M_j^l - M_j^\infty) \le l^{-1} 6c\rho^* (1 + 2c\rho^*)^{\frac{1}{2}} \ \text{ in } \Omega,$$

$$M_j^l - M_j^\infty = 0 \ \text{ on } \partial\Omega. \tag{2.19d}$$

Here, the L^∞ bound (2.7) has been used in the inequalities above. Let $v_k \in C^\infty(\Omega; \mathbb{R})$, $k = 1, 2$, be solutions of

$$\begin{cases} \dfrac{\mathrm{d}^2 v_1}{\mathrm{d}y^2} = 4\rho^*\left((\rho^*)^2 - 1\right) + c\,(1 + 2c\rho^*) & \text{in } \Omega, \\ \dfrac{\mathrm{d}^2 v_2}{\mathrm{d}y^2} = 6c\rho^*\,(1 + 2c\rho^*)^{\frac{1}{2}} & \text{in } \Omega, \\ v_k = 0 \quad \text{for } k = 1, 2 & \text{on } \partial\Omega. \end{cases}$$

Then each v_k only depends on the coupling parameter c. Hence, by the classical sub- and super-solution method, $l^{-1}v_1$ is a subsolution and $-l^{-1}v_1$ is a supersolution for each component of $(\mathbf{Q}^l - \mathbf{Q}^\infty)$, and similarly, $l^{-1}v_2$ is a subsolution and $-l^{-1}v_2$ is a supersolution for each of the vector components of $(\mathbf{M}^l - \mathbf{M}^\infty)$. The estimates then follow and the proof is complete. ∎

In the supplementary material, we compute asymptotic expansions for $\mathbf{Q}^l$, $\mathbf{M}^l$, for large l and small c, complemented by numerical experiments.

Next, we consider the $l \to 0$ limit for fixed c, which is valid for large channel widths D, much greater than the nematic correlation length. To this end, we rewrite the free energy (2.2) as

(2.20)
$$\frac{1}{l}F(Q_{11},Q_{12},M_1,M_2) \coloneqq \int_\Omega \left\{ \frac{1}{2}\left[\left(\frac{\mathrm{d}Q_{11}}{\mathrm{d}y}\right)^2 + \left(\frac{\mathrm{d}Q_{12}}{\mathrm{d}y}\right)^2\right] + \frac{1}{2}\left[\left(\frac{\mathrm{d}M_1}{\mathrm{d}y}\right)^2 + \left(\frac{\mathrm{d}M_2}{\mathrm{d}y}\right)^2\right] + \frac{1}{l}\bar{f}(Q_{11},Q_{12},M_1,M_2)\right\} \mathrm{d}y,$$

where

(2.21)
$$\bar{f}(Q_{11},Q_{12},M_1,M_2) \coloneqq \left(Q_{11}^2+Q_{12}^2-1\right)^2 + \frac{1}{4}\left(M_1^2+M_2^2-1\right)^2 - cQ_{11}\left(M_1^2-M_2^2\right) - 2cQ_{12}M_1M_2 - \alpha(c) \geq 0$$

and the c-dependent constant, $\alpha(c)$, is the minimum value of the bulk energy density. The set of minimizers of $\bar{f}$ plays a crucial role in the analysis, and belongs to the set

$$\mathcal{A}_{\min} \coloneqq \left\{(Q_{11},Q_{12},M_1,M_2) = \left(\rho^*\cos 2\phi, \rho^*\sin 2\phi, \sqrt{1+2c\rho^*}\cos\phi, \sqrt{1+2c\rho^*}\sin\phi\right)\right\},$$

where ρ^* is given by (2.8) and ϕ is an arbitrary angle (see the supplementary material (M140017SupMat.pdf [local/web 443KB])). The set $\mathcal{A}_{\min}$ is clearly a continuum.

Consider the following admissible test maps for sufficiently small l, with $Q_{12}^t(y) = M_2^t(y) \equiv 0$ for $y \in [-1,1]$ and

$$Q_{11}^t(y) = \begin{cases} g(y), & y \in \left[-1,-1+\sqrt{l}\right), \\ \rho^*, & y \in \left(-1+\sqrt{l},1-\sqrt{l}\right), \\ h(y), & y \in \left(1-\sqrt{l},1\right]. \end{cases}$$

Here, g linearly interpolates between ρ^* and $g(-1) = 1$; h linearly interpolates between ρ^* and $h(1) = -1$. Similarly, we use the following test map for M_1:

$$M_1^t(y) = \begin{cases} g^*(y), & y \in \left[-1,-1+\sqrt{l}\right), \\ \sqrt{1+2c\rho^*}, & y \in \left(-1+\sqrt{l},1-\sqrt{l}\right), \\ h^*(y), & y \in \left(1-\sqrt{l},1\right]. \end{cases}$$

Here, g^* linearly interpolates between $\sqrt{1+2c\rho^*}$ and $g^*(-1) = 1$; h^* linearly interpolates between $\sqrt{1+2c\rho^*}$ and $h^*(1) = -1$. We have $\bar{f}\left(\rho^*,0,\sqrt{1+2c\rho^*},0\right) = 0$ (also

see supplementary material (M140017SupMat.pdf [local/web 443KB])). It is then straightforward to check that

$$\frac{1}{l}F\left(Q_{11}^t, 0, M_1^t, 0\right) \leq \frac{C}{\sqrt{l}}$$

for a positive constant C independent of l with l small enough. Hence, for an energy minimizer $(\mathbf{Q}^l, \mathbf{M}^l)$ of the full energy (2.2), we necessarily have that

$$\frac{1}{l}F\left(Q_{11}^l, Q_{12}^l, M_1^l, M_2^l\right) \leq \frac{C}{\sqrt{l}},$$

and hence,

$$\int_{-1}^{1} \bar{f}\left(Q_{11}^l, Q_{12}^l, M_1^l, M_2^l\right)\ \mathrm{d}y \leq C\sqrt{l} \to 0 \quad \text{as } l \to 0.$$

Furthermore, since $\bar{f} \geq 0$ by its definition (2.21), we deduce that $\bar{f}(Q_{11}^l, Q_{12}^l, M_1^l, M_2^l) \equiv 0$ almost everywhere, as $l \to 0$. Hence, in the $l \to 0$ limit, we expect the energy minimizers, $\left(\mathbf{Q}^l, \mathbf{M}^l\right)$ to minimize the Dirichlet energy of $\mathbf{Q}$ and $\mathbf{M}$ in the constrained set $\mathcal{A}_{\min}$ defined above, so that the limiting minimizers are given by

(2.22)
$$\mathbf{Q}^0(c,y) = \rho^*(\cos(2\phi_0(y)), \sin(2\phi_0(y))),\ \mathbf{M}^0(c,y) = \sqrt{1+2c\rho^*}\,(\cos(\phi_0(y)), \sin(\phi_0(y)))\,,$$

where there are two choices of ϕ_0, dictated by the boundary conditions for $\mathbf{M}$:

$$\frac{\mathrm{d}^2\phi_0}{\mathrm{d}y^2} = 0, \tag{2.23a}$$

$$\phi_0(-1) = 0, \phi_0(1) = \pi \quad \text{or} \quad \phi_0(-1) = 0, \phi_0(1) = -\pi, \tag{2.23b}$$

$$2\phi_0 - \theta_0 = 2n\pi, \quad n \in \mathbb{Z}. \tag{2.23c}$$

Here, θ_0 and ϕ_0 denote the director and magnetization vector angles, respectively. In subsection 4.3, we numerically demonstrate that the energy minimizers, $\left(\mathbf{Q}^l, \mathbf{M}^l\right)$, indeed converge to one of the two limiting maps in $\mathcal{A}_{\min}$, defined above, almost everywhere except near $y = \pm 1$ (and interior points associated with the jumps in $(2\phi_0 - \theta_0)$, since $2\phi_0 - \theta_0$ is constrained to be an even multiple of 2π, in the $l \to 0$ limit). There are necessarily boundary layers near $y = \pm 1$, since the limiting maps in $\mathcal{A}_{\min}$ do not satisfy the boundary conditions at $y = \pm 1$. We indeed have multistability in this limit.

We do not prove convergence results in the $l \to 0$ limit rigorously, since this requires a delicate Γ-convergence analysis for a vector-valued problem with four degrees of freedom, with a continuum vacuum manifold, and additional complications from the boundary conditions. This warrants a separate study in its own right.

3. OR solutions. The results in section 2 concern the full problem (2.6a)–(2.6d) or ferronematic solutions with four degrees of freedom, $(\mathbf{Q}, \mathbf{M}) = (Q_{11}, Q_{12}, M_1, M_2)$. It is evident from the Euler–Lagrange equations (2.6a)–(2.6d), that we always have a branch of solutions with $Q_{12} = M_2 = 0$. We refer to such solutions with only two degrees of freedom, $(\mathbf{Q}, \mathbf{M}) = (Q_{11}, 0, M_1, 0)$ as OR solutions. A nematic (resp., magnetic) domain wall is defined to be a point $y = y^* \in (-1, 1)$ such that $\mathbf{Q}(y^*) = (Q_{11}(y^*), Q_{12}(y^*)) = 0$ (resp., $\mathbf{M}(y^*) = 0$). We call these points "walls" since they correspond to two-dimensional surfaces in the xz-plane. Ferronematic solutions need

not have domain walls in general but OR solutions in the admissible space (2.5) must have domain walls because of the imposed Dirichlet conditions. There must exist an interior point $y^* \in (-1,1)$ such that $Q_{11}(y^*) = 0$, because $Q_{11}(-1) = 1$ and $Q_{11}(1) = -1$, and $Q_{12}(y) = 0$ for all $y \in [-1,1]$ by definition; similar remarks apply to the domain wall in $\mathbf{M}$. Furthermore, domain walls in $\mathbf{Q}$ and $\mathbf{M}$ can occur at different points, as we shall see in section 4. OR solutions are special since the domain walls separate polydomains, i.e., distinctly ordered domains. In fact, recall the parameterization (2.11) and note that $Q_{12} = M_2 = 0$ implies $\theta = n\pi$ (for some integer n) everywhere; equivalent remarks apply to ϕ. Hence, there is necessarily a domain wall in $\mathbf{Q}$ such that $\theta = 2n\pi$ on one side of the domain wall containing $y = -1$, and $\theta = (2m+1)\pi$ (for some integers n, m) on the other side of the domain wall containing $y = 1$; analogously, there is a domain wall in $\mathbf{M}$ that separates two polydomains with $\phi = 2n\pi$ and $\phi = (2m+1)\pi$ for some integers n and m, respectively. These domain walls are associated with jumps in $\mathbf{n}$ and the normalised magnetisation vector, $\mathbf{m} = \mathbf{M}/|\mathbf{M}|$. The domain walls are not singularities of the $\mathbf{Q}$- and $\mathbf{M}$-solutions, although they regularize singularities/jumps in $\mathbf{n}$ and $\mathbf{m}$. Domain walls need not be associated with jumps and could just be regular zeroes of the $\mathbf{Q}$- and $\mathbf{M}$-fields, although such domain walls would be energetically expensive.

We interpret OR solutions as critical points of the following OR energy (which is equivalent to (2.2) with $Q_{12} = M_2 = 0$):

$$E(Q_{11}, M_1) \coloneqq \int_{-1}^{1} \left\{ \frac{l}{2}\left(\frac{\mathrm{d}Q_{11}}{\mathrm{d}y}\right)^2 + \frac{l}{2}\left(\frac{\mathrm{d}M_1}{\mathrm{d}y}\right)^2 + (Q_{11}^2 - 1)^2 + \frac{1}{4}\left(M_1^2 - 1\right)^2 - cQ_{11}M_1^2 \right\} \mathrm{d}y, \tag{3.1}$$

subject to the boundary conditions

$$Q_{11}(-1) = M_1(-1) = 1, \quad Q_{11}(1) = M_1(1) = -1, \tag{3.2}$$

in the admissible space

$$\mathcal{A}' = \left\{ Q_{11}, M_1 \in W^{1,2}(\Omega; \mathbb{R}), Q_{11} \text{ and } M_1 \text{ satisfy the boundary conditions (3.2)} \right\}. \tag{3.3}$$

The OR bulk energy density is given by:

$$f^{OR}(Q_{11}, M_1) = (Q_{11}^2 - 1)^2 + \frac{1}{4}(M_1^2 - 1)^2 - cQ_{11}M_1^2. \tag{3.4}$$

Hence, OR solutions are classical solutions of the following coupled ordinary differential equations:

$$\begin{aligned} l\frac{\mathrm{d}^2 Q_{11}}{\mathrm{d}y^2} &= 4Q_{11}(Q_{11}^2 - 1) - cM_1^2, \\ l\frac{\mathrm{d}^2 M_1}{\mathrm{d}y^2} &= M_1(M_1^2 - 1) - 2cQ_{11}M_1. \end{aligned} \tag{3.5}$$

In general, we expect multiple OR solutions for fixed values of (l, c) and the optimal OR solution is a minimizer of the energy (3.1) in $\mathcal{A}'$. We give a straightforward existence theorem below, which follows immediately from the direct method in the calculus of variations [14], along with some qualitative properties.

THEOREM 3.1 (existence, uniqueness, and maximum principle). *For all values of (l, c), there exists a minimizer, (Q_{11}^*, M_1^*) of the OR energy (3.1) in $\mathcal{A}'$. This OR minimizer, $(\mathbf{Q}^{OR}, \mathbf{M}^{OR}) = (Q_{11}^*, 0, M_1^*, 0)$, is a solution of the full system (2.6a)–(2.6d), and thus a critical point of the full energy (2.2). Additionally, $(\mathbf{Q}^{OR}, \mathbf{M}^{OR})$ is the unique critical point, and hence, global minimizer of the energy (2.2), for fixed positive c and l large enough, as in Theorem 2.5. Moreover, we have*

$$|Q_{11}(y)| \leq \rho^*, \ M_1^2(y) \leq 1 + 2c\rho^* \quad \forall y \in [-1, 1], \tag{3.6}$$

where ρ^* is given by (2.8).

Proof. Clearly, the admissible space $\mathcal{A}'$ is nonempty as $(Q_{11}, M_1) = (-y, -y) \in \mathcal{A}'$. We observe that (3.1) is lower semicontinuous since it is quadratic and thus, convex in both the gradients of Q_{11} and M_1 [14]. As before, the coupling energy density can be decomposed as follows, for arbitrary $\epsilon > 0$

$$-cQ_{11}M_1^2 \geq -\frac{c}{2}\left(\epsilon Q_{11}^2 + \frac{1}{\epsilon}M_1^4\right).$$

Therefore, the OR energy density is bounded from below, since f^{OR} is quartic in Q_{11} and M_1 and can absorb the terms above, for a suitable choice of ϵ. The existence of a minimizer, (Q_{11}^*, M_1^*), of the OR energy (3.1), is immediate from [14]. Furthermore, this minimizer is a (classical) solution of (3.5) subject to the boundary conditions (3.2). It is straightforward to check that the resulting OR solution, $\left(\mathbf{Q}^{OR}, \mathbf{M}^{OR}\right) = (Q_{11}^*, 0, M_1^*, 0)$, is also a solution of the full system, (2.6a)–(2.6d) in the admissible space (2.5) for all values of (l, c).

Since the full energy (2.2) has a unique critical point for l large enough (see Remark 2.6), we deduce that $\left(\mathbf{Q}^{OR}, \mathbf{M}^{OR}\right)$ is the unique energy minimizer of (2.2) in the $l \to \infty$ limit. The bounds (3.6) follow immediately from Theorem 2.3, using the L^∞ bounds for $|\mathbf{Q}|$ and $|\mathbf{M}|^2$ with $Q_{12} = M_2 = 0$. The solution branch $\left(\mathbf{Q}^{OR}, \mathbf{M}^{OR}\right)$ exists for all values of (l, c). This completes the proof. ∎

3.1. Convergence analysis in the $l \to 0$ limit. Now, we study the regime of small l, which describes macroscopic domains with $D \gg \sqrt{\frac{L}{|A|c^2}}$, for fixed $c > 0$. We define the set of minimizers of the OR bulk potential (3.4):

$$\mathcal{B}^{OR} = \left\{(Q_{11}, M_1) = \left(\rho^*, \sqrt{1 + 2c\rho^*}\right), (Q_{11}, M_1) = \left(\rho^*, -\sqrt{1 + 2c\rho^*}\right)\right\}.$$

As for the full problem, we expect minimizers of the OR energy (3.1) to converge to the set $\mathcal{B}^{OR}$ almost everywhere, away from $y = \pm 1$. In fact, the boundary conditions, $(Q_{11}(-1), M_1(-1)) = (1, 1)$ and $(Q_{11}(1), M_1(1)) = (-1, -1)$, do not belong to $\mathcal{B}^{OR}$, thus, OR energy minimizers must have boundary layers near $y = \pm 1$ in this limit. We make these heuristics more precise using Γ-convergence results, as in [28].

Consider the rescaled OR energy

$$\frac{1}{\sqrt{l}}E(Q_{11}, M_1) \coloneqq \int_{-1}^{1}\left\{\frac{\sqrt{l}}{2}\left(\frac{\mathrm{d}Q_{11}}{\mathrm{d}y}\right)^2 + \frac{\sqrt{l}}{2}\left(\frac{\mathrm{d}M_1}{\mathrm{d}y}\right)^2 + \frac{1}{\sqrt{l}}\tilde{f}(Q_{11}, M_1)\right\}\,\mathrm{d}y \tag{3.7}$$

where

$$\tilde{f}(Q_{11}, M_1) \coloneqq \left(Q_{11}^2 - 1\right)^2 + \frac{1}{4}\left(M_1^2 - 1\right)^2 - cQ_{11}M_1^2 - \beta(c) \geq 0, \tag{3.8}$$

and the c-dependent constant, $\beta(c)$, is the minimum value of the OR bulk potential. As in [6] and [28], we let $\mathbf{p} = (Q_{11}, M_1)$ and define the following metric d in the $\mathbf{p}$-plane, for any two points $\mathbf{p}_0, \mathbf{p}_1 \in \mathbb{R}^2$:

$$d(\mathbf{p}_0, \mathbf{p}_1) = \inf \left\{ \int_{-1}^{1} \tilde{f}^{1/2}(\mathbf{p}(t)) \left| \frac{\mathrm{d}\mathbf{p}(t)}{\mathrm{d}t} \right| \mathrm{d}t : \mathbf{p}(t) \in C^1\left([-1,1]; \mathbb{R}^2\right), \right. \\ \left. \mathbf{p}(-1) = \mathbf{p}_0, \mathbf{p}(1) = \mathbf{p}_1 \right\}. \tag{3.9}$$

This metric is degenerate as $\tilde{f}(\mathbf{p}) = 0$ for $\mathbf{p} = \mathbf{p}^* = \left(\rho^*, \sqrt{1 + 2c\rho^*}\right)$ and $\mathbf{p} = \mathbf{p}^{**} = \left(\rho^*, -\sqrt{1 + 2c\rho^*}\right)$. Despite such degeneracy, the infimum in (3.9) is indeed attained for arbitrary $\mathbf{p}_0$ and $\mathbf{p}_1$ (see [6, Lemma 9] and [28]). Denote $\mathbf{p}_b(1) = (-1, -1)$ and $\mathbf{p}_b(-1) = (1, 1)$. Let $\mathbf{p}_l$ be a minimizer of (3.7) for a fixed $c > 0$. A straightforward application of [28, Proposition 4.1] yields the following theorem.

THEOREM 3.2. *There exists a subsequence $l_k \to 0$ such that the minimizers $\mathbf{p}_{l_k}$ of (3.7) converge in $L^1([-1,1])$ almost everywhere to a map of the form $\mathbf{p}_0 = \sum_{j=1}^{N} p^j \chi_{E_j}$, where for any j, either $p^j = p^*$ or $p^j = p^{**}$, χ is the characteristic function of an interval, $E_j \subset (-1,1)$ such that $\cup_{j=1}^{N} E_j = (-1,1)$. Moreover, the intervals E_j minimize the following functional,*

$$J[E_j] := \sum_{j=1}^{N-1} d(\mathbf{p}^*, \mathbf{p}^{**}) + d(\mathbf{p}_0, \mathbf{p}_b(-1)) + d(\mathbf{p}_0, \mathbf{p}_b(1)), \tag{3.10}$$

where the first term describes the number of jumps between $\mathbf{p}^*$ and $\mathbf{p}^{**}$, referred to as interior transition layers that necessarily contain a magnetic domain wall, and the energetic costs of the boundary layers are captured by the second and third terms.

We compute the following transition costs,

$$d(\mathbf{p}^*, \mathbf{p}^{**}), d(\mathbf{p}^*, \mathbf{p}_b(1)), d(\mathbf{p}^{**}, \mathbf{p}_b(-1)), d(\mathbf{p}^*, \mathbf{p}_b(-1)), d(\mathbf{p}^{**}, \mathbf{p}_b(1)). \tag{3.11}$$

using the metric (3.9), and we can see from Figure 1 that

$$d(\mathbf{p}^*, \mathbf{p}_b(-1)) < d(\mathbf{p}^{**}, \mathbf{p}_b(-1)) < d(\mathbf{p}^{**}, \mathbf{p}_b(1)) < d(\mathbf{p}^*, \mathbf{p}^{**}) < d(\mathbf{p}^*, \mathbf{p}_b(1)).$$

It is clear that the minimizer of J in (3.10) is $\mathbf{p}^*$, with boundary layers near the edges $y = \pm 1$ and no interior jumps between $\mathbf{p}^*$ and $\mathbf{p}^{**}$.

3.2. Stability of OR solutions. The authors in [19] and [12] consider a similar OR problem with $c = 0$, in a one-dimensional channel and a two-dimensional square, respectively. In both cases, the OR solution loses stability as l decreases, or equivalently as the physical channel width D increases, with respect to perturbations that have nonzero Q_{12}. This motivates us to expect a similar instability result in the ferronematic setting with $c > 0$.

THEOREM 3.3 (instability of the OR solution). *For sufficiently small l and a fixed positive c, the OR energy minimizer, $(\mathbf{Q}^{OR}, \mathbf{M}^{OR})$, is an unstable critical point of (2.2), in the admissible space (2.5).*

Proof. For the OR solution $(\mathbf{Q}^{OR}, \mathbf{M}^{OR}) = (Q_{11}^*, 0, M_1^*, 0)$, we note that (Q_{11}^*, M_1^*) is a minimizer of the OR energy (3.1). Furthermore, the OR solution depends on l

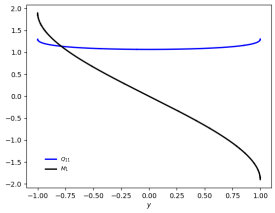
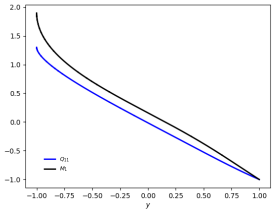
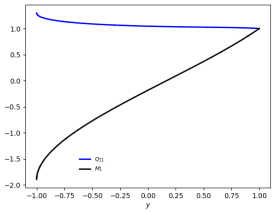

$d(\mathbf{p}^*, \mathbf{p}^{**}) \approx 3.008.$ $d(\mathbf{p}^*, \mathbf{p}_b(1)) \approx 3.967.$ $d(\mathbf{p}^{**}, \mathbf{p}_b(-1)) \approx 2.577.$

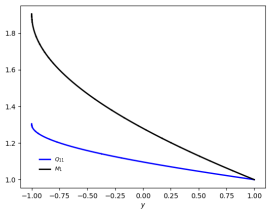
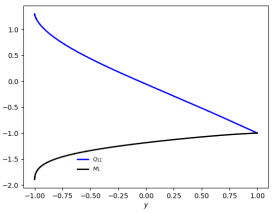

$d(\mathbf{p}^*, \mathbf{p}_b(-1)) \approx 0.455.$ $d(\mathbf{p}^{**}, \mathbf{p}_b(1)) \approx 2.591.$

FIG. 1. *The profiles of* $\mathbf{p}$ *and their corresponding transition costs in* (3.11).

with fixed $c > 0$ and we suppress this explicit dependence for brevity. We compute the second variation of the free energy (2.2) about $\left(\mathbf{Q}^{OR}, \mathbf{M}^{OR}\right)$ with arbitrary perturbations,

$$\tilde{Q}_{11}(y) = Q_{11}^*(y) + tg(y),\ \tilde{Q}_{12}(y) = th(y),$$
$$\tilde{M}_1(y) = M_1^*(y) + tv(y),\ \tilde{M}_2(y) = tw(y).$$

Here, $t \in \mathbb{R}$ and $g(y) = h(y) = v(y) = w(y) = 0$ at $y = \pm 1$. The second variation is then given by

$$\begin{aligned}\delta^2 F[g,h,v,w] &:= \frac{\mathrm{d}^2}{\mathrm{d}t^2}\bigg|_{t=0} F(\tilde{Q}_{11}, \tilde{Q}_{12}, \tilde{M}_1, \tilde{M}_2)\\ &= \delta^2 E[g,v] + \int_{-1}^{1} \left\{ l\left(\frac{\mathrm{d}h}{\mathrm{d}y}\right)^2 + l\left(\frac{\mathrm{d}w}{\mathrm{d}y}\right)^2 + 4h^2((Q_{11}^*)^2 - 1)\right.\\ &\quad \left. + w^2((M_1^*)^2 - 1) + 2cw^2 Q_{11}^* - 4chwM_1^* \right\} \mathrm{d}y\\ &=: \delta^2 E[g,v] + H[h,w],\end{aligned} \tag{3.12}$$

where $\delta^2 E[g,v]$ is the second variation of the OR energy (3.1) about (Q_{11}^*, M_1^*), and thus necessarily nonnegative for all admissible (g,v). To demonstrate the instability of $(\mathbf{Q}^{OR}, \mathbf{M}^{OR})$, we need to construct nontrivial h and w such that $H[h,w] < 0$. To this end, we follow methods in [19] and choose

$$h(y) = \frac{\mathrm{d}Q_{11}^*}{\mathrm{d}y} z(y) =: \tau(y) z(y), \qquad w(y) = \frac{\mathrm{d}M_1^*}{\mathrm{d}y} z(y) =: \zeta(y) z(y), \tag{3.13}$$

where z is a smooth cutoff function with bounded derivatives (independent of l) and $z(y) = 0$ for $|y| > 1 - \eta$, $0 < \eta < \frac{1}{4}$. Since h and w vanish at $y = \pm 1$, we have

$$\int_{-1}^{1} \left(h'\right)^2 \mathrm{d}y = -\int_{-1}^{1} hh'' \mathrm{d}y \quad \text{and} \quad \int_{-1}^{1} \left(w'\right)^2 \mathrm{d}y = -\int_{-1}^{1} ww'' \mathrm{d}y.$$

Here and hereafter, we take $'$ (resp., $''$) to denote the first (resp., second) derivative with respect to y. Furthermore, one can check from (3.5) that

(3.14)
$$\tau' = \frac{1}{l}\left[4Q_{11}^*\left((Q_{11}^*)^2-1\right)-c(M_1^*)^2\right], \quad \tau'' = \frac{1}{l}\left[4\tau\left(3(Q_{11}^*)^2-1\right)-2cM_1^*\zeta\right],$$
$$\zeta' = \frac{1}{l}\left[M_1^*\left((M_1^*)^2-1\right)-2cQ_{11}^*M_1^*\right], \quad \zeta'' = \frac{1}{l}\left[\zeta\left(3(M_1^*)^2-1\right)-2cM_1^*\tau-2cQ_{11}^*\zeta\right].$$

Now noting $h'' = \tau''z + 2\tau'z' + \tau z''$, $w'' = \zeta''z + 2\zeta'z' + \zeta z''$, and substituting (3.13) and (3.14) into $H[h,w]$, we obtain

$$\begin{aligned} H[h,w] &= \int_{-1}^{1}\left\{-8(Q_{11}^*)^2\tau^2z^2+2\zeta^2z^2\left(2cQ_{11}^*-(M_1^*)^2\right)\right\}\,\mathrm{d}y \\ &\quad + l\int_{-1}^{1}\left\{-2zz'\tau\tau'-2zz'\zeta\zeta'\right\}\,\mathrm{d}y + \int_{-1}^{1}\left\{-lzz''\left(\tau^2+\zeta^2\right)\right\}\,\mathrm{d}y \\ &=: \quad H_1+H_2+H_3. \end{aligned} \tag{3.15}$$

The Γ-convergence result in Theorem 3.2 implies that for an interior interval $(a,b)\subset[-1,1]$, it holds that

$$\int_a^b |Q_{11}^*-\rho^*|\,\mathrm{d}y \to 0 \quad \text{and} \quad \int_a^b \left|(M_1^*)^2-1-2c\rho^*\right|\,\mathrm{d}y \to 0 \quad \text{as } l\to 0. \tag{3.16}$$

We use integration by parts to obtain (recall that $l\int_{-1}^{1}\tau^2+\zeta^2 dy \le C\sqrt{l}$ as $l\to 0$ from the work in section 2.2)

$$\int_{-1}^{1}\left\{zz'\tau\tau'+zz'\zeta\zeta'\right\}\,\mathrm{d}y = -\frac{1}{2}\int_{-1}^{1}\left\{\left(z'\right)^2\left(\tau^2+\zeta^2\right)+zz''\left(\tau^2+\zeta^2\right)\right\}\,\mathrm{d}y,$$

so that $H_2\to 0$ as $l\to 0$. Moreover, it is straightforward to see that the third integral H_3 in (3.15) vanishes in the $l\to 0$ limit. It remains to estimate the first integral in (3.15). By (3.16), we deduce that

$$H_1 \to \int_{-1}^{1}\left\{-8\tau^2z^2\left(\rho^*\right)^2-2\zeta^2z^2\right\}\,\mathrm{d}y < 0 \quad \text{as } l\to 0. \qquad \square$$

4. Numerical results. In this section, we perform numerical experiments to validate our theoretical results and understand the interplay between l and c for the solution landscapes, with fixed $\xi = 1$. For the visualization, we plot the director $\mathbf{n}$ as rods and the normalized magnetization vector field $\mathbf{m} = \frac{\mathbf{M}}{|\mathbf{M}|}$ as arrows.

4.1. Solver details. Since the boundary-value problem is nonlinear, we use Newton's method with L^2 linesearch [8, Algorithm 2] as the outer nonlinear solver. The nonlinear solver is deemed to have converged when the Euclidean norm of the residual falls below 10^{-8}, or reduces from its initial value by a factor of 10^{-6}, whichever comes first. For the inner solver, the linearized systems are solved using the sparse LU factorization library MUMPS [1]. The solver described above is implemented in the *Firedrake* [25] library, which relies on PETSc [2] for solving the resulting linear systems. Furthermore, we use the *deflation* technique as described in [16] to compute multiple solutions and bifurcation diagrams. Throughout this section, we partition the

whole interval $[-1,1]$ into 1000 equidistant subintervals and numerically approximate the solutions using $\mathbb{P}^1$ finite elements (piecewise linear continuous polynomials).

Code availability. For reproducibility and more details of the implementation, we have archived the solver code [29] and the exact version of Firedrake [17] used to produce the numerical results of this work. An installation of Firedrake with components matching those used in this paper can be obtained by following the instructions at https://www.firedrakeproject.org/download.html with

```
python3 firedrake-install --doi 10.5281/zenodo.4449535
```

Defcon version #aaa4ef should then be installed, as described in https://bitbucket.org/pefarrell/defcon/.

4.2. OR solutions. We have analyzed the OR solution branch with $Q_{12} = M_2 = 0$, as $l \to 0$ and as $l \to \infty$. The OR branch is fully characterized by solutions of the boundary-value problem (3.5). OR solutions are special since they must contain separate domain walls in $\mathbf{Q}$ and $\mathbf{M}$, which can be tailored by varying l and c.

As $l \to \infty$, recall Theorem 3.1 to deduce that the OR solution branch is approximately given by $\left(\mathbf{Q}^{OR}, \mathbf{M}^{OR}\right) \approx (-y, 0, -y, 0)$, for a fixed c, and that $\left(\mathbf{Q}^{OR}, \mathbf{M}^{OR}\right)$ is also the unique minimizer of both the OR energy (3.1) and the full energy (2.2). In Figure 2, we plot the OR solution of (3.5) for $c = 1$ and $l = 10$. The profile is indeed linear, and we do not numerically obtain any other solutions, supporting the uniqueness result in the $l \to \infty$ limit. The OR solution vanishes at the channel center $y = 0$, i.e., $Q_{11}(0) = M_1(0) = 0$, and thus both the nematic and magnetic domain walls coincide at $y = 0$. Therefore, the normalized magnetization vector $\mathbf{m}$ and director $\mathbf{n}$ have a jump discontinuity at $y = 0$, i.e., $\mathbf{m}$ jumps from $\mathbf{m} = (1, 0)$ for $y < 0$ to $\mathbf{m} = (-1, 0)$ for $y > 0$, while $\mathbf{n}$ jumps from $\mathbf{n} = (1, 0)$ (modulo a sign) for $y < 0$ to $\mathbf{n} = (0, 1)$ (modulo a sign) for $y > 0$. We also plot the pointwise L^∞ bound (3.6) as blue solid lines in Figure 2, and this bound is indeed respected.

As $l \to 0$, for fixed $c > 0$, we expect $Q_{11} \to \rho^*$ and $M_1^2 \to 1 + 2c\rho^*$ uniformly away from $y = \pm 1$, for the OR energy minimizer in (3.1). We note that $\rho^*(c)$ defined in (2.8) is an increasing function of c and $\rho^*(0) = 1$, thus $\rho^*(c) > 1$ for all $c > 0$. As discussed in Theorem 3.2, we expect a domain wall in $\mathbf{Q}$ near the edge $y = 1$, within a boundary layer of width $\sqrt{l}$, where Q_{11} jumps from $Q_{11} = \rho^* > 1$ to $Q_{11}(1) = -1$. Hence, there necessarily exists a nematic domain wall with $Q_{11} = 0$, within this boundary layer close to $y = 1$. Analogously, there is a boundary layer near the other end point $y = -1$, within which Q_{11} jumps from $Q_{11}(-1) = 1$ to $Q_{11} = \rho^*$, but this boundary layer does not contain a nematic domain wall. Moreover, we expect that there are at least two minimizers of the OR energy (3.1) for l small enough, with opposite signs of M_1 in the channel interior. Each of these minimizers must contain

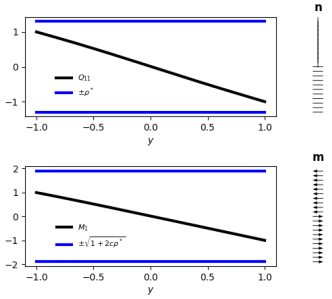

FIG. 2. *The only (stable) solution of* (3.1) *for* $c = \xi = 1$ *and* $l = 10$.

at least one magnetic domain wall: near $y = 1$ if $M_1 > 0$ in the interior, or near $y = -1$ if $M_1 < 0$ in the interior, respectively. In what follows, a transition layer refers to a thin interval within which M_1 jumps between $-\sqrt{1+2c\rho^*}$ and $\sqrt{1+2c\rho^*}$ and each of these transition layers necessarily contains a magnetic domain wall with $M_1 = M_2 = 0$. We expect the OR energy (3.1) to have multiple critical points, with multiple interior transition layers and domain walls in $\mathbf{Q}$ and $\mathbf{M}$, for l small enough. However, we only expect two OR energy minimizers, that have the same Q_{11} profile but differ in the sign of M_1, and the nematic and magnetic domain walls do not occur at the same point. Of course, all OR solutions are unstable critical points of the full energy (2.2) for l small enough, as proven in Theorem 3.3. We now numerically corroborate these theoretical conjectures with $l = 0.01$ and $\xi = 1$.

In Figure 3, we present four example solutions with $c = 1$. In fact, they are all unstable critical points of the full energy (2.2) whilst being stable critical points of the OR energy (3.1) (in the sense that the Hessian of the second variation of the OR energy about these critical points has positive eigenvalues). As expected, these solution profiles, (Q_{11}, M_1), have boundary layers near the endpoints. Furthermore, interior transition layers in M_1 (near the center $y = 0$) are observed in Solutions 3 and 4. The L^∞ bounds (3.6) (blue solid line) for $|Q_{11}|$ and $|M_1|$ are also satisfied.

In Figure 4, we plot the stable solutions of the OR energy (3.1) for a larger value $c = 5$, which are unstable critical points of the full energy (2.2). Indeed, each of the solutions in Figure 4 has one unstable eigendirection, in the context of the full energy (2.2). The two profiles in Figure 4, have boundary layers near $y = \pm 1$, and essentially

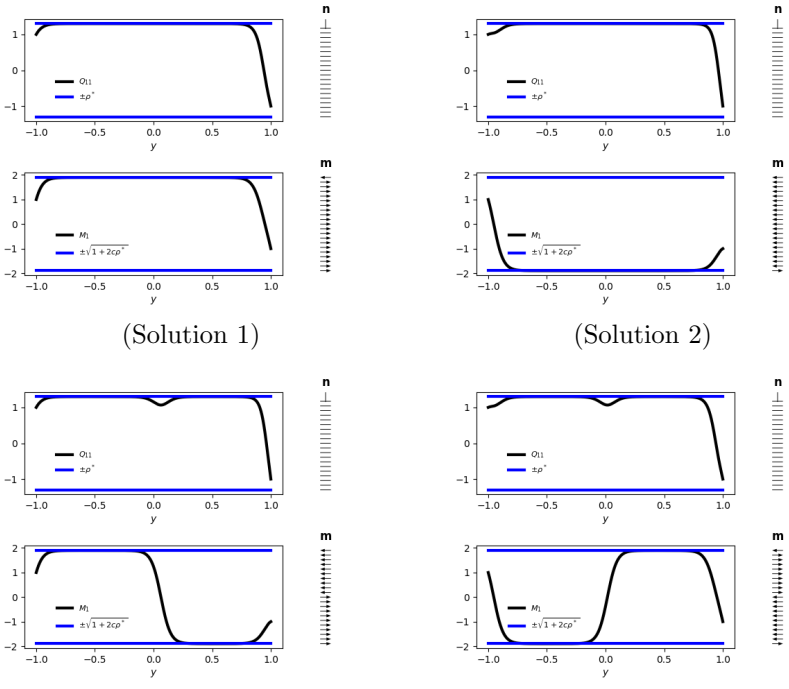

FIG. 3. *Four stable OR critical points of* (3.1)*, with* $c = \xi = 1$ *and* $l = 0.01$*. Solution* 1 *is the minimizer of the OR energy* (3.1).

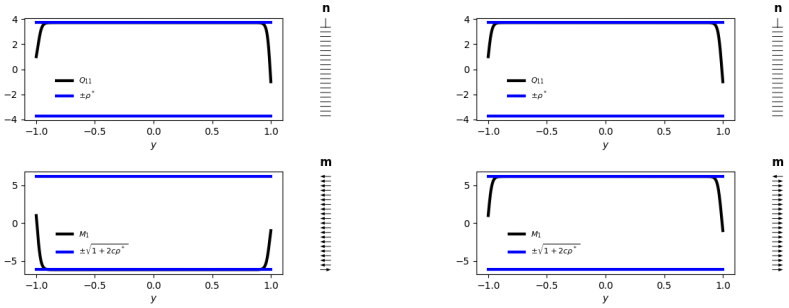

FIG. 4. *Two stable OR critical points of* (3.1)*, for* $c = 5$*,* $\xi = 1$*, and* $l = 0.01$*. The right profile has lower OR energy than the left profile and the solutions in Figure* 5*.*

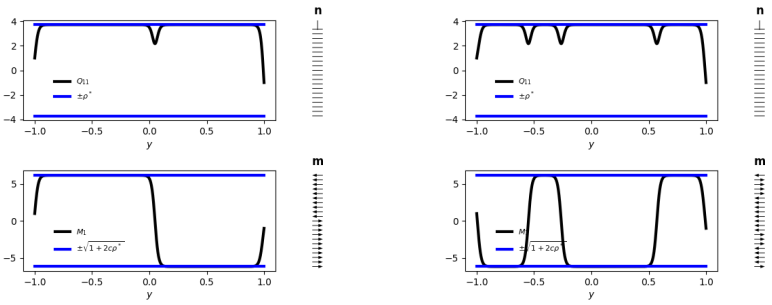

FIG. 5. *Two stable OR critical points of* (3.1)*, with single (left) and multiple (right) interior transition layers for* $c = 5$*,* $\xi = 1$*, and* $l = 0.01$*. The left has lower OR energy.*

differ in the sign of M_1 in the interior; Q_{11} only vanishes near $y = 1$ as predicted by the Γ-convergence analysis, so that we have a nematic domain wall near $y = 1$. On the other hand, M_1 can vanish either near $y = -1$ or near $y = 1$, so that the corresponding magnetic domain wall can occur near either boundary. Additionally, there are other solutions with interior transition layers for M_1; see two examples in Figure 5 where single and multiple interior transition layers in M_1 are observed. They are also stable critical points of the OR energy (3.1). The transition layers in M_1 necessarily contain a magnetic domain wall with $M_1 = 0$, and these interior magnetic domain walls are not accompanied by associated nematic domain walls. Moreover, solutions with interior transition layers have higher OR energy (3.1) than solutions without interior transition layers in Figure 4, since each transition layer has an energetic cost of $d(\mathbf{p}^*, \mathbf{p}^{**})$ as explained in Theorem 3.2.

These numerical experiments illustrate that we can manipulate the location and multiplicity of nematic and magnetic domain walls in the OR solutions by varying l, e.g., the domain walls in the OR energy minimizers migrate from the channel center to the channel boundaries at $y = \pm 1$, as l decreases.

4.3. Solutions of the full problem. Next, we consider the full problem (2.6a)–(2.6d) with four degrees of freedom, $(Q_{11}, Q_{12}, M_1, M_2)$. We only consider the case of small $l_1 = l_2 = l = 0.01$ with $\xi = 1$, since the OR solution branch is the unique solution of the full problem, in the $l \to \infty$ limit.

In Figure 6, we take $c = 1$ and present four examples of stable solutions with four degrees of freedom. We also plot the L^∞ bound (2.7) in the figures, illustrating that Theorem 2.3 is indeed satisfied. There are no interior domain walls with $|\mathbf{Q}| = |\mathbf{M}| = 0$

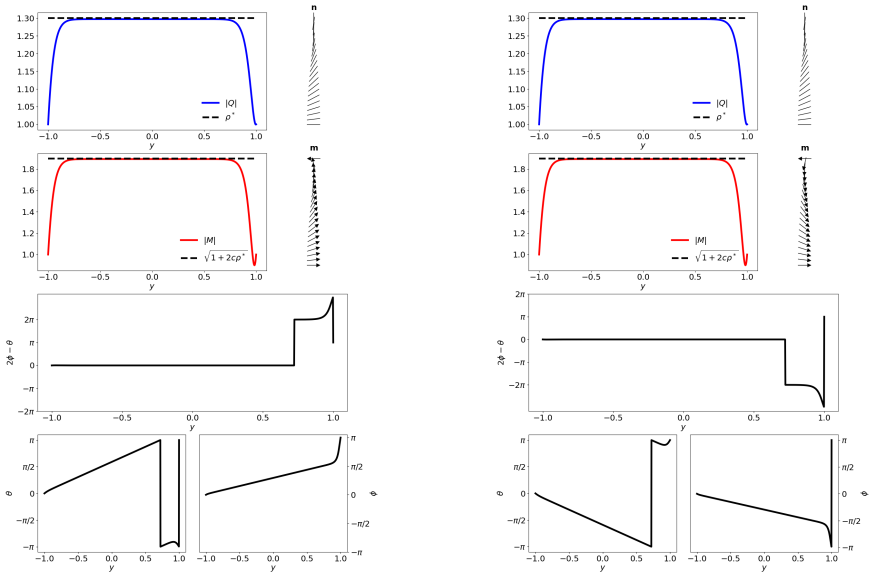

(Solution 1; stable) (Solution 2; stable)

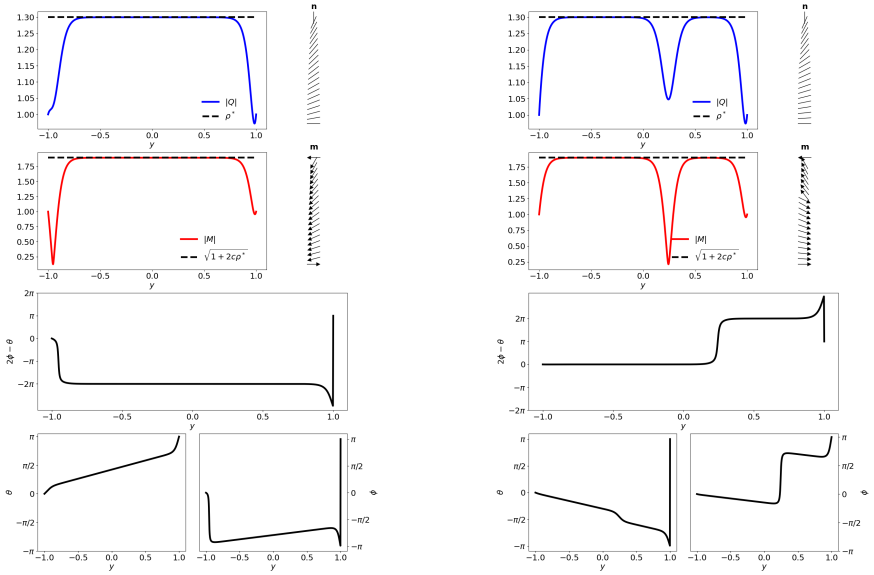

(Solution 3; stable) (Solution 4; stable)

FIG. 6. *Four stable stationary profiles,* $(Q_{11}, Q_{12}, M_1, M_2)$*, of* (2.2) *with* $l = 0.01$ *and* $c = \xi = 1$*, along with plots of* $(2\phi - \theta)$*,* θ*, and* ϕ *to verify the relation* (2.23)*. Solutions* 1 *and* 2 *have the lowest full energy value* (2.2)*.*

for small l, as discussed in subsection 2.2. Furthermore, Solutions 1, 2, and 3 in Figure 6 only have boundary layers, with almost constant $|\mathbf{Q}|-, |\mathbf{M}|$-profiles in the domain interior, whereas Solution 4 has interior nonzero local minima in $|\mathbf{Q}|$ and $|\mathbf{M}|$. Solutions 1 and 2 are the energy minimizers while the remaining two profiles are nonminimizing stable critical points of the full energy (2.2). Note that the two energy minimizers differ in their $\mathbf{m}$-patterns (more precisely, the sign of M_2). Moreover, we

compute the values of θ, ϕ defined to be

$$\theta = \arctan\left(\frac{Q_{12}}{Q_{11}}\right), \quad \phi = \arctan\left(\frac{M_2}{M_1}\right) \tag{4.1}$$

for each solution. It can be seen that $|\mathbf{Q}| \to \rho^*$ and $|\mathbf{M}|^2 \to 1 + 2c\rho^*$ for the energy minimizer (Solution 1), whereas $(2\phi - \theta)$ tends to an even multiple of π almost everywhere, except near $y = \pm 1$. We do not attempt to explain the interior jumps in the plots of $(2\phi - \theta)$, except that these jumps will have a distinct optical signature in physical experiments. Furthermore, the separate plots of θ and ϕ demonstrate linear behavior except around the local minima of $|\mathbf{Q}|$ or $|\mathbf{M}|$ and the boundary layers, consistent with the limiting Laplace equation (2.23) for ϕ and θ in the $l \to 0$ limit.

Now, we repeat the simulations for $c = 5$. Two stable stationary profiles are illustrated in Figure 7. We see that $|\mathbf{Q}| \to \rho^*$ and $|\mathbf{M}|^2 \to 1 + 2c\rho^*$ almost everywhere, as expected. Here, Solution 2 has lower energy than Solution 1, since Solution 1 has more local minima in $|\mathbf{Q}|$ and $|\mathbf{M}|$ than Solution 2. Further, $(2\phi - \theta)$ is an even multiple of π almost everywhere, with the jumps being associated with the local minima in $|\mathbf{Q}|$ and $|\mathbf{M}|$, thus verifying (2.23c). Additionally, we plot ϕ and θ in Figure 7, and observe almost linear profiles, except around the local minima and boundary layers. To summarize, the numerical experiments and the heuristics in section 2.2 suggest that there are at least two energy minimizers, characterized by $(\rho_1, \sigma_1, \theta_1, \phi_1)$ and $(\rho_2, \sigma_2, \theta_2, \phi_2)$ of (2.2) in the $l \to 0$ limit, such that $\rho_1, \rho_2 \to \rho^*$, $\sigma_{1,2}^2 \to 1 + 2c\rho^*$ almost everywhere away from $y = \pm 1$, $\theta_2 = -\theta_1$, $\phi_2 = -\phi_1$, with no domain walls and $2\phi_{1,2} - \theta_{1,2}$ an even multiple of π except near $y = 1$. The two energy minimizers differ in their sense of rotation, in $\mathbf{n}$ and $\mathbf{m}$, between $y = \pm 1$.

4.4. Bifurcation diagram with continuing l. We vary $l_1 = l_2 = l \in [0.2, 3.0]$ with step size 0.01 and $c = 1$ in Figure 8. There is only one stable OR solution for

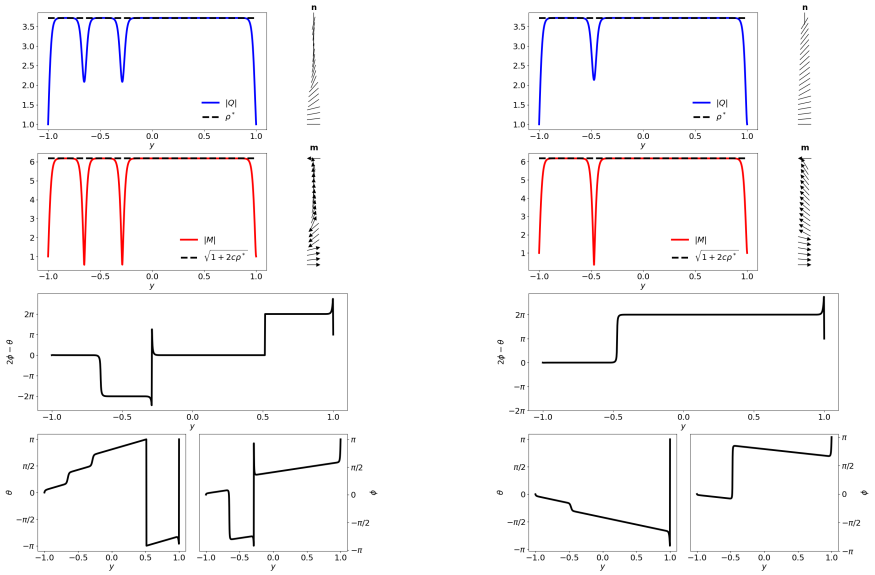

(Solution 1; stable) (Solution 2; stable)

FIG. 7. *Two examples of stable stationary profiles* $(Q_{11}, Q_{12}, M_1, M_2)$ *of the full energy* (2.2) *with* $l = 0.01$, $c = 5$, *and* $\xi = 1$. *Solution* 2 *has lower energy than Solution* 1.

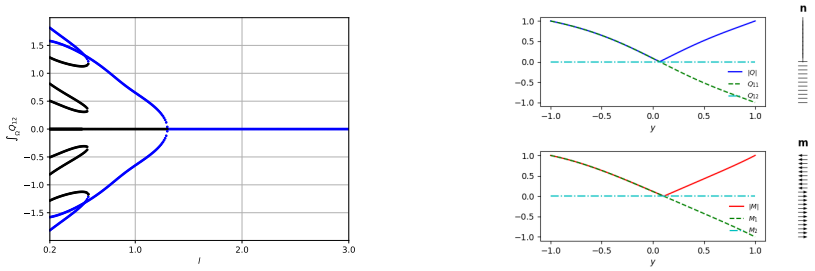

FIG. 8. *Left: the bifurcation diagram of continuing* $l_1 = l_2 = l \in [0.2, 3.0]$ *with fixed* $c = \xi = 1$*; here, black represents unstable solutions while blue indicates stable solutions. Right: the stable solution for* $l = 2$*.*

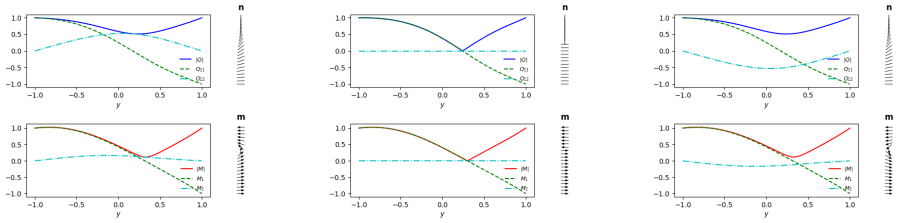

(Solution 1; stable) (Solution 2; unstable) (Solution 3; stable)

FIG. 9. *Three solutions for* $l = 1$ *in Figure* 8*. Solutions* 1 *and* 3 *are global energy minimizers.*

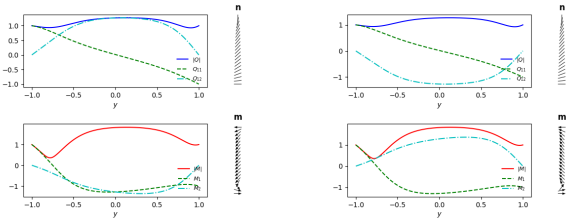

(Solution 1; stable) (Solution 4; stable)

FIG. 10. *Two examples of new stable solutions for* $l = 0.2$ *in Figure* 8*. They are global energy minimizers.*

$l \in [1.25, 3.0]$, it being the energy minimizer of the full energy (2.2). For $l \approx 1.25$, there is a pitchfork bifurcation consisting of two stable solution branches and one unstable OR branch (also see Figure 9). In fact, the two stable solutions (Solutions 1 and 3 in Figure 9) differ by the sign of Q_{12} and M_2, i.e., for every solution branch, $(Q_{11}, Q_{12}, M_1, M_2)$, there exists another solution branch with $(Q_{11}, -Q_{12}, M_1, -M_2)$. The stable solution branches correspond to a smooth rotation in $\mathbf{n}$, between $y = \pm 1$ and are actually the global energy minimizers for $l \leq 1.25$.

As l becomes smaller, more (stable or unstable) solutions are found. More specifically, there are four disconnected bifurcations appearing around $l = 0.55$, giving two further stable solutions, which are also local energy minimizers (see Figure 10 for an illustration) for $l \in [0.2, 0.55]$. Again, they only differ by the sign of Q_{12} and M_2. In Figure 10, we plot two examples of newly found stable solution profiles. The stable solutions typically correspond to smooth $\mathbf{n}$-profiles with minimal rotation (minimal

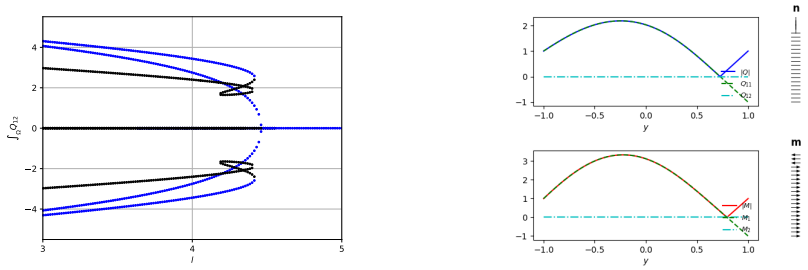

FIG. 11. *Left: the bifurcation diagram with fixed* $c = 5$ *and* $\xi = 1$*; here, black labels unstable solutions while blue labels stable solutions. Right: one stable OR solution for* $l = 4.45$.

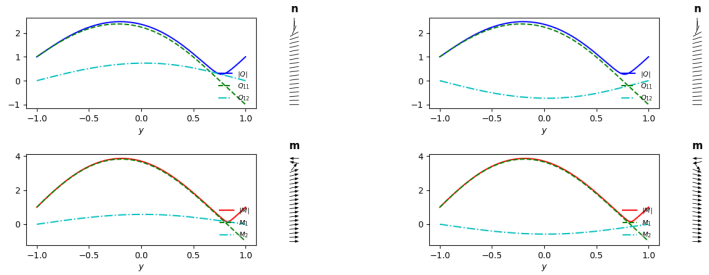

FIG. 12. *Two new stable solutions at* $l = 4.43$ *in Figure* 11.

topological degree consistent with the boundary conditions), while the stable normalized magnetization profiles $\mathbf{m}$ are also smooth, except near $y = \pm 1$.

We next consider the case of $c = 5$, by numerically computing a bifurcation diagram in Figure 11, for the solutions of (2.6a)–(2.6d), by continuing $l \in [3, 5]$ with a step size of 0.015. The globally stable OR solution is shown in Figure 11 and it loses stability at the pitchfork bifurcation point $l \approx 4.44$, leading to two new stable branches (see illustrations in Figure 12 for $l = 4.43$). The new stable solutions only differ in the signs of Q_{12} and M_2 and are, in fact, energy minimizers for $l \leq 4.34$. Thus, the qualitative features of the bifurcation diagram are unchanged by increasing c, but the OR solution branch loses stability for $l < l^*(c)$, where $l^*(c)$ is an increasing function of c. Hence, as c increases, OR solutions are increasingly difficult to find owing to their shrinking window of stability.

Remark 4.1. We comment on the two folds in the bifurcation diagram Figure 11. They do not represent the same solution branch at the intersection points. Instead, they are just overlapping points in this plot of $\int_\Omega Q_{12}$ versus l. A different functional may yield a bifurcation diagram without these intersection points.

5. Conclusions. We study confined systems with both nematic and magnetic orders, inside a channel geometry with Dirichlet boundary conditions. Specifically, we model the stable equilibria as minimizers of an appropriately defined energy on an interval $[-D, D]$, with three contributions: a nematic energy, a magnetic energy, and a nemato-magnetic coupling energy. We are interested in two parameters: the scaled elastic parameter l that is inversely proportional to D^2, and the nemato-magnetic coupling parameter c. We rigorously show that c reduces the effective nematic correlation length ξ_n, for large c, and we have the unique OR solution for $D \ll \frac{c^*}{c}\xi_n$, for some explicitly computable constant c^*, independent of c. The OR solution necessar-

ily has separate nematic and magnetic domain walls, which are surface defects. As D increases for fixed c (or c increases for fixed D), there can be multiple OR solutions, all of which are unstable with varying locations and multiplicities of domain walls, and the stable solutions do not have domain walls or polydomains for large D. There are multiple stable solutions for large D, characterized by the rotation profiles of $\mathbf{n}$ and $\mathbf{m}$ between the boundaries. Our choice of boundary conditions necessarily leads to boundary layers, which again will have distinct optical signatures, if implemented. We have provided analytic characterizations of the limiting profiles for small D (in terms of the OR solution) and large D (in terms of limiting maps) accompanied by extensive numerical studies, which beautifully illustrate how we can use l and c to tune domain walls, boundary layers, and multistability, all of which can be exploited for optical and mechanical responses. This work gives informative insight into the complex interplay between geometry, material properties, temperature (captured by l), nemato-magnetic coupling, and boundary conditions in the solution landscapes (also see [21] for the numerical analysis of this system). Our methods can be modified to include different types of boundary conditions and nemato-magnetic coupling, which could enhance the stability of OR solutions, and we will develop universal theoretical frameworks for composite materials with multiple order parameters in future work.

Acknowledgment. The authors thank Giacomo Canevari for helpful discussions regarding the stability of OR solutions.

REFERENCES

[1] P. R. Amestoy, I. Duff, and J.-Y. L'Excellent, *Multifrontal parallel distributed symmetric and unsymmetric solvers*, Comput. Methods Appl. Mech. Engrg., 184 (2000), pp. 501–520.

[2] S. Balay, S. Abhyankar, M. F. Adams, J. Brown, P. Brune, K. Buschelman, L. Dalcin, V. Eijkhout, W. D. Gropp, D. Kaushik, M. Knepley, L. C. McInnes, K. Rupp, B. F. Smith, and H. Zhang, *PETSc Users Manual*, Technical report ANL-95/11 - Revision 3.9, Argonne National Laboratory, Argoane, IL, 2018.

[3] F. Bethuel, H. Brezis, and F.Hélein, *Asymptotics for the minimization of a Ginzburg–Landau functional*, Calc. Var. Partial Differental Equations, 1 (1993), pp. 123–148.

[4] K. Bisht, V. Banerjee, P. Milewski, and A. Majumdar, *Magnetic nanoparticles in a nematic channel: A one-dimensional study*, Phys. Rev. E (3), 100 (2019), 012703.

[5] K. Bisht, Y. Wang, V. Banerjee, and A. Majumdar, *Tailored morphologies in two-dimensional ferronematic wells*, Phys. Rev. E (3), 101 (2020), 022706.

[6] A. Braides, *A handbook of Γ-convergence*, in Handbook of Differential Equations: Stationary Partial Differential Equations, Vol. 3, Elsevier, Amsterdam, 2006, pp. 101–213.

[7] F. Brochard and P. G. de Gennes, *Theory of magnetic suspensions in liquid crystals*, J. Phys. France, 31 (1970), pp. 691–708.

[8] P. R. Brune, M. G. Knepley, B. F. Smith, and X. Tu, *Composing scalable nonlinear algebraic solvers*, SIAM Rev., 57 (2015), pp. 535–565, https://doi.org/10.1137/130936725.

[9] S. V. Burylov and Y. L. Raikher, *Macroscopic properties of ferronematics caused by orientational interactions on the particle surfaces.* I. *Extended continuum model*, Mol. Cryst. Liq. Cryst. Sci. Technol. Sect. A, 258 (1995), pp. 107–122.

[10] M. C. Calderer, A. DeSimone, D. Golovaty, and A. Panchenko, *An effective model for nematic liquid crystal composites with ferromagnetic inclusions*, SIAM J. Appl. Math., 74 (2014), pp. 237–262.

[11] G. Canevari, J. Harris, A. Majumdar, and Y. Wang, *The well order reconstruction solution for three-dimensional wells, in the Landau–de Gennes theory*, Internal. J. Nonlinear Mech., 119 (2020), 103342.

[12] G. Canevari, A. Majumdar, and A. Spicer, *Order reconstruction for nematics on squares and hexagons: A Landau–de Gennes study*, SIAM J. Appl. Math., 77 (2017), pp. 267–293.

[13] P. G. de Gennes, *The Physics of Liquid Crystals*, Oxford University Press, Oxford, 1974.

[14] L. C. Evans, *Partial Differential Equations*, 2nd ed., Grad. Stud. Math. 19, American Mathematical Society, Providence, RI, 2010.

[15] L. Fang, A. Majumdar, and L. Zhang, *Surface, size and topological effects for some nematic equilibria on rectangular domains*, Math. Mech. Solids, 25 (2020), pp. 1101–1123.

[16] P. E. Farrell, Á. Birkisson, and S. W. Funke, *Deflation techniques for finding distinct solutions of nonlinear partial differential equations*, SIAM J. Sci. Comput., 37 (2015), pp. A2026–A2045.

[17] Firedrake-Zenodo, *Software Used in this Manuscript*, https://doi.org/10.5281/zenodo.4449535 (2021).

[18] J. P. F. Lagerwall and G. Scalia, *A new era for liquid crystal research: Applications of liquid crystals in soft matter nano-, bio- and microtechnology*, Curr. Appl. Phys, 12 (2012), pp. 1387–1412.

[19] X. Lamy, *Bifurcation analysis in a frustrated nematic cell*, J. Nonlinear Sci., 24 (2014), pp. 1197–1230.

[20] Q. Liu, P. J. Ackerman, T. C. Lubensky, and I. I. Smalyukh, *Biaxial ferromagnetic liquid crystal colloids*, Proc. Natl. Acad. Sci. USA, 113 (2016), pp. 10479–10484.

[21] R. R. Maity, A. Majumdar, and N. Nataraj, *Parameter dependent finite element analysis for ferronematics solutions*, 103 Comput. Math. Appl., (2021), pp. 127–55.

[22] A. Majumdar, *Equilibrium order parameters of nematic liquid crystals in the Landau–de Gennes theory*, European. J. Appl. Math, 21 (2010), pp. 181–203.

[23] A. Majumdar and A. Zarnescu, *Landau-de Gennes theory of nematic liquid crystals: The Oseen–Frank limit and beyond*, Arch. Ration. Mech. Anal, 196 (2010), pp. 227—-280.

[24] A. Mertelj, D. Lisjak, M. Drofenik, and M. Čopič, *Ferromagnetism in suspensions of magnetic platelets in liquid crystals*, Nature, 504 (2013), pp. 237–241.

[25] F. Rathgeber, D. A. Ham, L. Mitchell, M. Lange, F. Luporini, A. T. T. McRae, G. T. Bercea, G. R. Markall, and P. H. J. Kelly, *Firedrake: Automating the finite element method by composing abstractions*, ACM Trans. Math. Software, 43 (2017), pp. 1–27.

[26] J. Rault, P. E. Cladis, and J. P. Burger, *Ferronematics*, Phys. Lett. A, 32 (1970), pp. 199–200.

[27] I. W. Stewart, *The Static and Dynamic Continuum Theory of Liquid Crystals: A Mathematical Introduction*, Taylor & Francis, London, 2004.

[28] Y. Wang, G. Canevari, and A. Majumdar, *Order reconstruction for nematics on squares with isotropic inclusions: A Landau–de Gennes study*, SIAM J. Appl. Math., 79 (2019), pp. 1314–1340.

[29] J. Xia, *Ferronematics-Numerics*, https://doi.org/10.5281/zenodo.4616745 (2021).